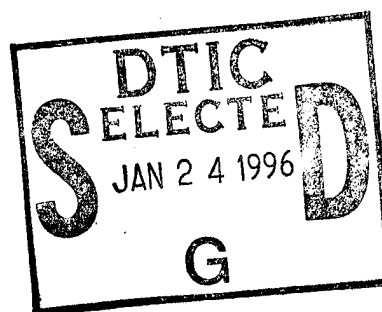# NAVAL POSTGRADUATE SCHOOL
MONTEREY, CALIFORNIA

THESIS

AN EVALUATION OF THE EFFECTS OF
OPTICAL KLYSTRONS ON THE SELENE
FREE ELECTRON LASER OSCILLATOR

by

Eric A. Kelsey

June, 1995

Thesis Advisor: William B. Colson

Approved for public release; distribution is unlimited.

REPORT DOCUMENTATION PAGE			Form Approved OMB No. 0704-0188

Public reporting burden for this collection of information is estimated to average 1 hour per response, including the time for reviewing instruction, searching existing data sources, gathering and maintaining the data needed, and completing and reviewing the collection of information. Send comments regarding this burden estimate or any other aspect of this collection of information, including suggestions for reducing this burden, to Washington Headquarters Services, Directorate for Information Operations and Reports, 1215 Jefferson Davis Highway, Suite 1204, Arlington, VA 22202-4302, and to the Office of Management and Budget, Paperwork Reduction Project (0704-0188) Washington DC 20503.

1. AGENCY USE ONLY *(Leave blank)*	2. REPORT DATE June, 1995	3. REPORT TYPE AND DATES COVERED Master's Thesis	
4. TITLE AND SUBTITLE AN EVALUATION OF THE EFFECTS OF OPTICAL KLYSTRONS ON THE SELENE FREE ELECTRON LASER OSCILLATOR		5. FUNDING NUMBERS	
6. AUTHOR(S) Eric A. Kelsey			
7. PERFORMING ORGANIZATION NAME(S) AND ADDRESS(ES) Naval Postgraduate School Monterey CA 93943-5000		8. PERFORMING ORGANIZATION REPORT NUMBER	
9. SPONSORING/MONITORING AGENCY NAME(S) AND ADDRESS(ES)		10. SPONSORING/MONITORING AGENCY REPORT NUMBER	

11. SUPPLEMENTARY NOTES The views expressed in this thesis are those of the author and do not reflect the official policy or position of the Department of Defense or the U.S. Government.

12a. DISTRIBUTION/AVAILABILITY STATEMENT Approved for public release; distribution is unlimited.	12b. DISTRIBUTION CODE

13. ABSTRACT *(maximum 200 words)*

Lasers have been incorporated into many parts of society including heavy industrial work, military defense, light displays, scientific research, and everyday household appliances. Free Electron Lasers (FELs) use relativistic electrons traveling in an alternating magnetic field to produce coherent radiation. One particular application for a FEL is to beam power to satellites. The United States and Russia have agreed to pursue this effort together. The installation in the United States is the SpacE Laser ENErgy (SELENE) project scheduled for installation at China Lake, California.

The SELENE laser system consists of an oscillator and a radiator. The electrons are bunched in the oscillator in preparation for entering the radiator. The use of a three-section optical klystron has been proposed for the SELENE oscillator. An optical klystron FEL is composed of multiple undulator sections, each separated from the next by a dispersive section. This dispersive section allows for larger gain from a shorter total length of undulator. The effects of the optical klystrons in the SELENE oscillator using the proposed SELENE FEL parameters will be investigated through the use of simulations of two and three-section undulators.

14. SUBJECT TERMS Free Electron Lasers, Lasers, Optical Klystrons, SELENE.			15. NUMBER OF PAGES 93
			16. PRICE CODE
17. SECURITY CLASSIFICATION OF REPORT Unclassified	18. SECURITY CLASSIFICATION OF THIS PAGE Unclassified	19. SECURITY CLASSIFICATION OF ABSTRACT Unclassified	20. LIMITATION OF ABSTRACT UL

AN EVALUATION OF THE EFFECTS OF OPTICAL KLYSTRONS ON THE SELENE FREE ELECTRON LASER OSCILLATOR

Eric A. Kelsey

Lieutenant, United States Navy

B. S., University of Mississippi, 1988

Submitted in partial fulfillment of the

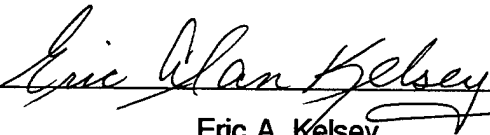requirements for the degree of

MASTER OF SCIENCE IN PHYSICS
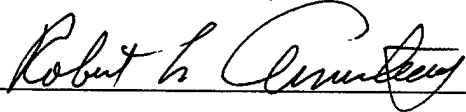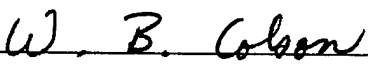
from the

NAVAL POSTGRADUATE SCHOOL

June 1995

Author: _____

Eric A. Kelsey

Approved by: _____

William B. Colson, Thesis Advisor

_____

Robert L. Armstead, Second Reader

_____

William B. Colson, Chairman,

Department of Physics

iii

ABSTRACT

Lasers have been incorporated into many parts of society including heavy industrial work, military defense, light displays, scientific research, and everyday household appliances. Free Electron Lasers (FELs) use relativistic electrons traveling in an alternating magnetic field to produce coherent radiation. One particular application for a FEL is to beam power to satellites. The United States and Russia have agreed to pursue this effort together. The installation in the United States is the SpacE Laser ENErgy (SELENE) project scheduled for installation at China Lake, California.

The SELENE laser system consists of an oscillator and a radiator. The electrons are bunched in the oscillator in preparation for entering the radiator. The use of a three-section optical klystron has been proposed for the SELENE oscillator. An optical klystron FEL is composed of multiple undulator sections, each separated from the next by a dispersive section. This dispersive section allows for larger gain from a shorter total length of undulator. The effects of the optical klystrons in the SELENE oscillator using the proposed SELENE FEL parameters will be investigated through the use of simulations of two and three section undulators.

Accesion For		
NTIS CRA&I	☒	
DTIC TAB	☐	
Unannounced	☐	
Justification		
By		
Distribution /		
Availability Codes		
Dist	Avail and / or Special	
A-1		

TABLE OF CONTENTS

ACKNOWLEDGEMENT

I. INTRODUCTION

The United States and the Russian governments have agreed to a joint venture to investigate the possibilities of using a Free Electron Laser (FEL) to provide electrical power to satellites from a ground based system [1]. This project was started in Novosibirsk, Russia. The initial prototype of the system is to be built and tested at Novosibirsk at an output power of 200 kW. The United States has proposed the SpacE Laser ENErgy (SELENE) system to be built at China Lake, California. This system has a designed output of 10 MW.

The concepts which generated the need for the SELENE system have been around since the early days of the space program. One of the dominant factors is the cost per kilogram to place a satellite in a stable orbit, which can be as high as $160,000 per kilogram for a geosynchronous orbit [1]. This consideration forces the payload to be mass efficient. Some of the payload must be used for the power and orbital maintenance systems. The power systems consist of large solar panels used to collect sunlight and convert it to electricity, and battery backup systems used to store the energy for use when the satellite is in a blackout period. The orbital maintenance systems generally consist of chemically powered thrusters used to maintain a geosynchronous orbit. Due to the limited supply of chemical fuel for the thrusters, the satellite- has a limited time to maintain orbit. The continuous bombardment of micrometeors subject the solar panels and connectors to physical stresses which will render them inoperable. The continuous deep charge and discharge cycle of the battery system will also limit battery lifetime. Thus, due to power considerations, satellites have a limited lifetime, considering the cost to place them into orbit. With the large number of satellites and satellite-supported systems in the military today, a means of reducing the cost of placing satellites into orbit and extending their lifetimes would be of great benefit. For example, it would allow increased functional payload,

1

more numerous, smaller satellites for greater area coverage, or significant cost savings which could be used for technological research.

The effect SELENE will have on satellite lifetimes and payload is tremendous, especially if a system of similar lasers systems is installed globally to provide coverage for all satellites. Continuous coverage for all geosynchronous satellites over the United States may be achieved with three stations. With the use of a beacon satellite to direct the beam to individual satellites, all Low Earth Orbit satellites in the Western Hemisphere north of the equator can receive power from SELENE located at China Lake, California. [2]

The current solar cells used in satellites are inefficient. The use of silicon photocells is common in most satellites. These cells receive broad-band solar radiation and convert 10-15% of the incident radiation to electricity for use by the satellite [2]. Using the SELENE project to tune the light to a wavelength near the peak sensitivity of the current silicon cells can improve the overall conversion efficiency by a factor of three. The capability of focusing the laser on the solar cells will increase the incident intensity on the solar cells by a factor of 4.6 allowing for smaller arrays of photocells to achieve the same power production. Using the current silicon based solar cells, this represents a gain of almost 14 in power output per unit area of solar panel. With SELENE, the solar cells can be designed for an optimum wavelength for electrical conversion improving the conversion efficiency by a factor of four. These smaller arrays will reduce the weight, as well as the cross-sectional area of the satellite. This will reduce the number of interactions the satellite has with micrometeors which will enhance the reliability of the satellite's power systems.

The chemical propulsion systems required for station keeping may also be replaced with a system of electrically powered, ion thruster propelled, satellite tugs. These tugs can be used to precisely place the satellite in the exact orbit required for them to perform their mission. This will remove the problem of fuel supply exhaustion as well as removing the large mass required by the chemical boosters and storage

2

systems. With these changes in standard satellite design, the mass of the support systems on the satellite and the cost per kilogram to orbit will be reduced. The return on satellite lifetime is large, considering the expense of placing a single satellite in orbit multiplied by the enormous number of satellites available. This innovative system will have a cost return of almost ten to one. [1].

The SELENE project design is unique in its three-section undulator. The purpose of the dual dispersive sections in the undulator is to provide additional flexibility in the design and operation of the FEL, as well as to reduce the steady-state optical field strength in the oscillator. The separate oscillator and radiator sections are necessary to provide bunching of the electrons in a weak optical field prior to their entering the radiator. This allows for large power output from the radiator, which does not require optical devices, while keeping the power density low in the oscillator to minimize damage to the optical devices in the system. The beam from the radiator then travels through an underground vacuum tube where it expands sufficiently for the mirrors to project it to the satellites with minimal mirror damage.

II. FREE ELECTRON LASER THEORY

A. INTRODUCTION

The basic design of an FEL oscillator, shown in Fig. 1, consists of a relativistic electron beam, a wiggler, and an oscillator cavity. The wiggler, or undulator, consists of a series of periodic magnetic fields either in a linear configuration or in a helical pattern. The helical undulator is more efficient at transferring energy from the electrons to the optical field, but the linear configuration is much easier and less expensive to construct. Most operating FEL's today use a linear undulator. The oscillator consists of two mirrors, one of which is completely reflective and the other is partially reflective to allow optical power to be extracted.

Due to the transverse acceleration provided by the magnetic fields in the undulator, the electrons in the FEL emit radiation in a cone directed along the electron's velocity vector. The size of the cone is related to the velocity of the electrons. Some of this radiation is trapped by the oscillator and provides the optical field for interaction with following electrons. The interaction between the electrons, the magnetic field, and the optical field cause bunching in the electron beam on the scale of the optical wavelength of the FEL. This microscopic bunching produces coherent radiation and gain in the optical field. This is the basic principle behind the FEL.

With the large number of high energy electrons present in the electron beam and the relatively large acceleration produced by the undulator fields, the possibility of high output power is easily recognized. The frequency of the radiated light is proportional to the energy of the accelerating electrons, thus providing for coherent light which can be tuned over a wide range of frequencies. Some of the operating parameters of an FEL are the number, size and magnetic field strength of the undulator periods, the electron beam energy, current, and pulse shape, the quality of the electron beam, the transmission coefficient of the oscillator output mirror, the presence of special

5

undulator designs such as dispersive sections, length of the oscillator, and the radius of the mirrors. The effects these parameters have on FEL design and output characteristics will be studied, with emphasis on the effects of dispersive sections on high gain FELs.
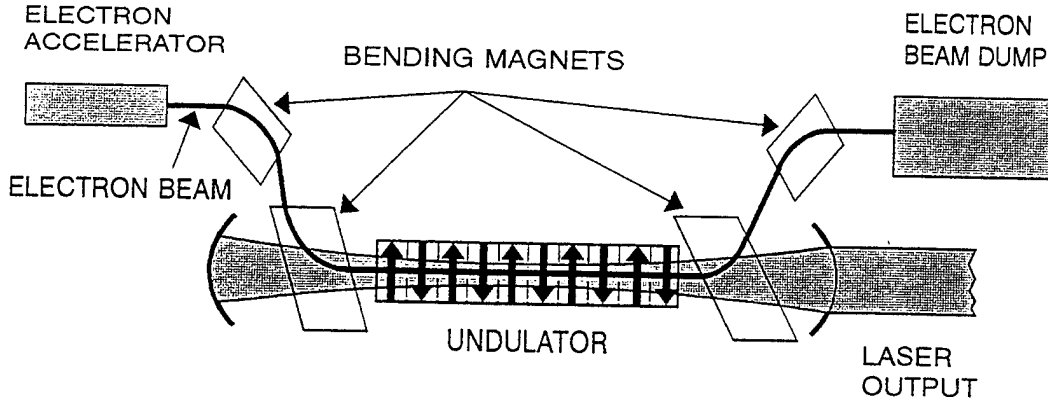
Figure 1. Elements of a typical FEL oscillator.

B. RADIATION FROM CHARGED PARTICLES

For a single electron, the Lienard-Wiechert potentials in SI units are [3],

$$\phi_{LW}(\vec{r},t) = \frac{e}{4\pi\varepsilon_0} \frac{1}{|\vec{s}(\vec{r},\tau_r)|} g(\vec{r},\tau_r) , \tag{2.1}$$

and

$$\vec{A}_{LW}(\vec{r},t) = \frac{e\mu_0}{4\pi} \frac{\vec{v}(\tau_r)}{|\vec{s}(\vec{r},\tau_r)|} g(\vec{r},\tau_r) , \tag{2.2}$$

where ϕ_{LW} is the electric field potential, $\vec{A}_{LW}$ is the vector potential, e is the charge on the electron, $\vec{s}(\vec{r},\tau_r)$ is the vector from the source point to the field point $\vec{r}$, τ_r is the retarded time at which the particle radiated in order for the radiation to reach $\vec{r}$ at time t, $\vec{v}(\tau_r)$ is the velocity of the electron at time τ_r, ε_0 is the permittivity of free space, μ_0 is the permeability of free space, and

6

$$g(\vec{r},\tau_r) = [1 - \frac{1}{c}\vec{n}(\vec{r},\tau_r) \cdot \vec{V}(\tau_r)]^{-1} \tag{2.3}$$

is the relativistic correction factor where c is the speed of light and $\vec{n}$ is the unit vector in the direction of $\vec{s}$. The electric ($\vec{E}$) and magnetic ($\vec{B}$) fields can be derived from Maxwell's equations,

$$\vec{B}(\vec{r},t) = \nabla \times \vec{A}_{LW}(\vec{r},t) \tag{2.4}$$

and

$$\vec{E}(\vec{r},t) = -\nabla \phi_{LW} - \frac{\partial}{\partial t}\vec{A}_{LW} . \tag{2.5}$$

Each field can be broken down into two components as shown below in Equations 2.6 and 2.7, one dependent on the velocity of the particle and the other proportional to the acceleration as denoted by the respective subscripts v and a. These field vectors are [3]

$$\vec{E}(\vec{r},t)=\vec{E}_v+\vec{E}_a \begin{cases} \vec{E}_v(\vec{r},t) = \dfrac{e\mu_0}{4\pi}\dfrac{g^3}{s^2}c^2\left[1-\dfrac{v^2}{c^2}\right]\left[\vec{n}-\dfrac{\vec{v}_1}{c}\right] \\[4mm] \vec{E}_a(\vec{r},t) = \dfrac{e\mu_0}{4\pi}\dfrac{g^3}{s}\vec{n}\times\left[\left[\vec{n}-\dfrac{\vec{v}}{c}\right]\times\vec{a}\right] \end{cases} , \tag{2.6}$$

and

$$\vec{B}(\vec{r},t) = \vec{B}_v+\vec{B}_a \begin{cases} \vec{B}_v = \dfrac{1}{c}\vec{n}\times\vec{E}_v \\[4mm] \vec{B}_a = \dfrac{1}{c}\vec{n}\times\vec{E}_a \end{cases} . \tag{2.7}$$

The electric field proportional to the acceleration, E_a, has a directional component $f(\theta,v)$, which can be defined as

7

$$f(\theta,v) \equiv \left| g^3 \left[\vec{n} - \frac{\vec{v}}{c} \right] \right| = \frac{\left[1 + \frac{\vec{v}^2}{c^2} - 2\frac{v}{c}\cos\theta \right]^{1/2}}{\left[1 - \frac{v}{c}\cos\theta \right]^3} , \tag{2.8}$$

where θ is the angle between $\vec{v}$ and $\vec{n}$. Looking in the direction of $\vec{v}$ where $\theta = 0$, $f(0,v) = (1-v/c)^{-2}$ which becomes very large as v approaches c. Thus, in the extreme relativistic limit, the radiation will normally be peaked in the direction of $\vec{v}$. This is not always the case as there are additional factors not noted above. Specifically, in the case that the acceleration is in the same direction as the velocity, $(\vec{n} - \vec{v}/c) \times \vec{a} = 0$ for a field point in the direction of $\vec{v}$, and there is no radiation emitted in the direction of $\vec{v}$. For the FEL, the undulator's magnetic field produces a force on the electron which is perpendicular to the motion of the electron and $f(\theta,\vec{v})$ is sufficient to describe the radiation pattern produced by a single electron.

Table 1 shows some typical ranges for the angular spread of the radiation pattern, in degrees, where $\theta'(x)$ is the angle where $f(\theta',v) = x\, f(0,v)$, T_e is the relativistic kinetic energy of the electron in MeV, and x is the ratio of the directional factor at the angle θ' to the maximum value of the directional factor at $\theta = 0$. For example, for an electron with $\gamma = 100$, the directional factor $f(\theta',v)$ falls to 90% of $f(0,v)$ at an angle of $\theta' = 2.5°$ from $\vec{v}$ as shown in bold type in Table 1. The Lorentz factor, $\gamma = (1 - \vec{\beta}^2)^{-1/2}$ where $\vec{\beta} = \vec{v}/c$, will be used extensively in the development of FEL theory since the electron beam is relativistic.

8

v/c	γ	T_e (MeV)	θ' (0.5) (degrees)	θ' (0.1) (degrees)	θ' (0.01) (degrees)
0.90000	2.29	.66	29.1	51.1	98.2
0.99000	7.09	3.1	13.1	20.1	34.1
0.99900	22.37	10.9	5.6	8.2	13.5
0.99990	70.71	35.6	2.3	3.3	5.4
0.99995	100.0	50.6	1.79	2.5	4.1
0.99999	223.6	114	.96	1.3	2.2

Table 1. Angular spread of the radiation from a relativistic electron. After Ref. [3].

C. ELECTRON INTERACTION WITH MAGNETIC FIELDS

The path taken by the electrons while in the undulator determines the FEL characteristics. The electrons are injected into the undulator at relativistic velocities and encounter the magnetic fields of the undulator, producing spontaneous radiation.

The magnetic field of the undulator is usually produced by permanent magnets or current carrying coils. The electrons are directed along the axis of the undulator, which will be represented as the z-axis. For linear undulators, the magnets will be aligned with the x-axis. When the electrons are injected into the undulator, they see the magnetic field as being Lorentz-contracted. In a helical undulator with circular polarization, the magnetic field in cylindrical coordinates (r,θ,z) is [4]

$$B_r^H = 2B_0 \left[I_0(k_0 r) - \frac{I_1(k_0 r)}{k_0 r} \right] \sin(\theta - k_0 z) \ ,$$

$$B_\theta^H = \left[\frac{2B_0}{k_0 r} \right] I_1(k_0 r) \cos(\theta - k_0 z), \text{ and} \tag{2.9}$$

$$B_z^H = -2B_0 I_1(k_0 r) \cos(\theta - k_0 z) \ ,$$

where B_0 is the peak magnetic field strength of the undulator, $k_0 = 2\pi/\lambda_0$ is the wave number of the undulator, and λ_0 is the length of one undulator period. I_0 and I_1 are hyperbolic Bessel functions [5]. Off the axis, it is the transverse components of Eq. 2.9 which act to modify the electrons trajectory along the undulator length. Near the axis, Eq. 2.9 may be expanded for $k_0 r \ll 1$ to find the increase in the average transverse magnetic field as r increases,

$$\bar{B}_\perp^H \approx B_0(1 + k_0^2 r^2/4 + \cdots) \ . \tag{2.10}$$

This higher magnetic field density away from the axis results in the electrons being funneled back towards the axis where the ideal on-axis magnetic field in rectangular coordinates is

$$\vec{B}^H = [B_x, B_y, B_z] = B_0[\cos(k_0 z), \sin(k_0 z), 0] \ . \tag{2.11}$$

The magnitude of the transverse magnetic field in an helical undulator, is constant along the z axis, $\bar{B}_\perp = B_0$. This allows for simpler analytical analysis of FEL interactions.

For a linear undulator, the on-axis magnetic field in rectangular coordinates [4] is

$$\vec{B}^L = B_0[0, \sin(k_0 z)\cosh(k_0 y), \cos(k_0 z)\sinh(k_0 y)] \tag{2.12}$$

and the increase in the average magnetic field strength as the electron moves off axis is

$$\bar{B}^L = \frac{B_0}{\sqrt{2}}(1 + k_0^2 y^2/2 + \cdots). \tag{2.13}$$

10

As can be seen by Eq. 2.13, the linear undulator provides for focusing in the y direction only. Radial focusing may be achieved using quadrupole lenses or by using magnetic poles with parabolic faces instead of flat faces [6]. The ideal magnetic field strength on axis for a linear undulator is

$$\vec{B}^L = B_0[0,\sin(k_0z),0],$$ (2.14)

and the average magnetic field strength seen by the electrons is $\bar{B}_\perp = B_0/\sqrt{2}$. This results in smaller acceleration in the transverse direction as compared with the helical undulator and thus reduced emissions, coupling and gain. The helical undulator naturally provides radial focusing without the added engineering required by the linear undulator. From the evidence presented, it would seem that the helical undulator design is superior in performance as compared to the linear undulator. However, the helical undulator uses current carrying coils for creating the magnetic field in the undulator whereas the linear undulator uses permanent magnets. Thus the cost of constructing and operating helical undulators results in the use of linear undulators in most modern FELs.

For an electron perfectly injected into an ideal linear undulator, using the Lorentz force equation in CGS units,

$$\frac{d\vec{p}}{dt} = \frac{d(mc\gamma\vec{\beta})}{dt} = q(\vec{E} + \vec{\beta} \times \vec{B}),$$ (2.15)

the magnetic field of (2.14), and assuming $\gamma \approx$ constant, results in

$$\dot{\beta}_x = \dot{\beta}_\perp = -\frac{q}{mc\gamma}\beta_z B_0 \sin(k_0z)$$

$$\dot{\beta}_y = 0$$ (2.16)

$$\dot{\beta}_z = \frac{q}{mc\gamma}\beta_x B_0 \sin(k_0z)$$

for equations of motion in the absence of an optical field, where m is the mass of the electron and $q = -e$ is the charge on the electron. Using $z = \beta_z ct$ and the

approximation $\beta_z \approx$ constant ≈ 1 together, it can be shown that

$$x = \frac{K}{\gamma k_0}\sin(k_0 ct), \text{ and}$$

(2.17)

$$\dot{x} = \beta_\perp c = \frac{Kc}{\gamma}\cos(k_0 ct) .$$

This gives a peak displacement in the x direction of $K/k_0\gamma$, where $K = eB_0\lambda_0/2\pi mc^2$ is the dimensionless FEL parameter. For a typical FEL, $\gamma = 100$, $e = 4.8\times10^{-10}$ statcoulombs, $m = 9.1\times10^{-28}$ gm, $\beta_z \approx 1$, $c = 3\times10^{10}$cm/s, $\lambda_0 = 5$ cm, $k_0 = 2\pi/\lambda_0 = 1.25$cm^{-1}, and $B_0 = 4$ kG , which results in $K \approx 1.87$ and a peak displacement in the x direction of 0.15 mm.

In order for the proper coupling between the electron beam and the optical field to occur, the electron beam should stay within the optical mode while in the undulator. From a basic study of optics, the distance over which an optical mode area doubles due to natural diffraction, called the Rayleigh length, is $z_0 = \pi w_0^2/\lambda$, where w_0 is the radius of the optical field at the waist. If the Rayleigh length is not matched to the undulator, the optimal coupling cannot occur. For example, if the Rayleigh length is much smaller than the undulator length, then the optical mode area will become much larger than the electron beam. This will result in reduced coupling for two reasons. First, the optical field strength will be reduced in amplitude since it will be spread over a larger optical mode area and second, the electrons will be interacting with a smaller fraction of the total mode area. Thus, the capability of the undulator and optical field to bunch the electrons and produce coherent radiation will be reduced. For a Rayleigh length equal to the length of the undulator, the optical mode area will be $\approx \lambda L$, which, for a typical FEL with $\lambda = 10$ µm and $L = 5$ m results in a mode radius of 4.0 mm. For a typical FEL, the wiggle motion of the electrons in the undulator remains inside the optical mode. The relative size of the electron beam with respect to the optical field is quantified by the filling factor $F = \pi r_b^2/\pi w_0^2$ where r_b is the radius of the electron beam.

D. ELECTRON INTERACTION WITH OPTICAL FIELDS

The interaction of the electrons with the light field determines the FEL's ability to produce coherent light. As the electrons travel through the undulator, they oscillate in the transverse direction once per undulator period. The electrons must move slower than the light in the undulator. When the change in relative position of the electrons and optical field is equal to one wavelength of light at the end of one undulator period, the electrons are at resonance [8]. Therefore $\lambda = c(1-\beta_z)\Delta t$ where λ is the wavelength of the light emitted at resonance, and $\Delta t = \lambda_0/c\beta_z$. Solving for β_z using the Lorentz factor, and $\beta_\perp^2 = K^2/\gamma^2$, results in $\beta_z \approx 1-(1+K^2)/2\gamma^2$. The resonance condition follows directly,

$$\lambda = \lambda_0 \frac{1+K^2}{2\gamma^2}. \tag{2.18}$$

This shows that the output frequency of the FEL can be tuned by changing the undulator parameters λ_0 or K, or more readily, by changing the electron beam energy, γmc^2.

The motion of the electrons in the undulator may be described by a simple pendulum equation as shown below. The plane electromagnetic wave propagating down a helical undulator may be described by [4]

$$\vec{E}_r = E(z,t)[\cos(\psi),-\sin(\psi),0]$$
$$\vec{B}_r = \hat{z}\times\vec{E} = E(z,t)[\sin(\psi),\cos(\psi),0] . \tag{2.19}$$

where $\psi = kz-\omega t+\phi$, $k = 2\pi/\lambda$, $\omega = kc$ is the angular frequency of the light, λ is the optical wavelength, ϕ is the phase of the light, and E is the magnitude of the optical wave. The behavior of the relativistic electrons in the presence of electromagnetic fields can be described using the Lorentz force equation, (Eq. 2.15) and the time rate of change of the energy of the electron,

$$\frac{d(\gamma mc^2)}{dt} = -ec\vec{\beta}\cdot\vec{E} , \tag{2.20}$$

where the energy of the electron is γmc^2. In total, the electron interacts with the fields $\vec{E} = \vec{E}_r$ and $\vec{B} = \vec{B}_0 + \vec{B}_r$. Solving the Lorentz force equation for $\beta_\perp$, assuming perfect injection into a helical undulator and $\beta_z \approx 1$ results in

$$\vec{\beta}_\perp = -\frac{K}{\gamma}[\cos(k_0 z), \sin(k_0 z), 0] .$$ (2.21)

Thus, inserting Eq. 2.21 and $\vec{E}_r$ from Eq. 2.19 into Eq. 2.20 gives

$$\dot{\gamma} = \frac{eEK}{\gamma mc}\cos(\zeta + \phi) ,$$ (2.22)

where the relative phase between the electron and the optical field is given by $\zeta = (k + k_0)z - \omega t$. For $-\pi/2 < \zeta + \phi < \pi/2$, $\dot{\gamma} > 0$ and energy is transferred from the optical field to the electrons, and for $\pi/2 < \zeta + \phi < 3\pi/2$, $\dot{\gamma} < 0$ and energy is transferred from the electron beam to the optical field. Now the effect of bunching becomes apparent. If the electrons are bunched near $\zeta + \phi = \pi$, then there will be a large fraction of electrons radiating energy to the optical field in the same phase and the optical field will grow. If the same group of electrons are bunched near $\zeta + \phi = 0$, then the electrons will be absorbing energy from the optical field and the optical field strength will decrease. If the electrons are evenly distributed in phase with respect to the light, then as many electrons will lose energy as will take energy from the optical field and the net change in optical field strength will be zero.

Using the definition of γ, Eq. 2.17, differentiating γ^{-2} with respect to t, and equating with Eq. 2.22, the fractional change per unit time in the energy of the electron is found to be

$$\frac{\dot{\gamma}}{\gamma} = \frac{\gamma^2 \beta_z \dot{\beta}_z}{1 + K^2} = \frac{eEK}{\gamma^2 mc}\cos(\zeta + \phi) .$$ (2.23)

Taking the second derivative of ζ with respect to time, solving for $\dot{\beta}_z$, and substituting the result into Eq. 2.23 gives

$$\frac{\gamma^2 \beta_z}{(1 + K^2)(k + k_0)c}\ddot{\zeta} = \frac{eEK}{\gamma^2 mc}\cos(\zeta + \phi) .$$ (2.24)

14

Using the resonance condition (Eq. 2.18), $\beta_z \approx 1$ and $k \gg k_0$ for $\gamma \gg 1$, the pendulum equation is found to be

$$\ddot{\zeta} = \frac{2k_0 eEK}{\gamma^2 m} \cos(\zeta + \phi) \,.$$

(2.25)

In order to simplify calculations and to get a scale that is valuable to compare different FEL designs, the use of dimensionless parameters is introduced. A dimensionless time, τ, is defined by

$$\tau \equiv \frac{\bar{\beta}_z ct}{L} \approx \frac{ct}{L}$$

(2.26)

where $L = N\lambda_0$ is the length of the undulator, N is the number of undulator periods and

$$\frac{d^2}{dt^2}(...) = \frac{c^2}{L^2}\frac{d^2}{d\tau^2}(...) = \frac{c^2}{L^2}(\overset{\circ\circ}{...}) \,.$$

(2.27)

This "normalizes" the FEL so that τ goes from 0 to 1 as the electrons travel down the undulator. The dimensionless pendulum equation for a helical undulator then becomes

$$\overset{\circ\circ}{\zeta} = \overset{\circ}{v} = \frac{4\pi NeKLE}{\gamma^2 mc^2} \cos(\zeta + \phi) = |a| \cos(\zeta + \phi)$$

(2.28)

where $|a|$ is the magnitude of the dimensionless optical field strength in the oscillator and $v = \overset{\circ}{\zeta}$ is the relative phase velocity between the optical field and the electron.

For a linear undulator, the electromagnetic radiation in the undulator is of the form [4],

$$\vec{E}_r(\vec{x},t) = E(z,t)[\cos(kz - \omega t + \phi(z,t)),0,0]$$

(2.29)

$$\vec{B}_r(\vec{x},t) = E(z,t)[0,\cos(kz - \omega t + \phi(z,t)),0] \,.$$

This radiation field, combined with the magnetic field of the linear undulator from Eq. 2.12, will result in a similar dimensionless pendulum equation,

15

$$\overset{\circ\circ}{\zeta} = \overset{\circ}{v} = \frac{4\pi NeK(J_0(\xi) - J_1(\xi))L}{\gamma^2 mc^2} \frac{E}{\sqrt{2}} \cos(\zeta + \phi) = |a| \cos(\zeta + \phi) \qquad (2.30)$$

where J_0 and J_1 are solutions to Bessel's differential equations, $\xi = K^2/2(1 + K^2)$, and $K = eB_0\lambda_0/\sqrt{2}2\pi mc^2$ is the rms undulator parameter.

E. OPTICAL WAVE DEVELOPMENT

To see how the optical fields develop and interact with the electron beam, the derivation starts with Maxwell's equations in CGS units. The relationship between the vector potential, $\vec{A}(\vec{r},t)$, and the current density perpendicular to the direction of propagation of the optical field, $\vec{J}_\perp(\vec{r},t)$ as functions of position, $\vec{r}$ and time, t, can be used to derive

$$\left[\vec{\nabla}^2 - \frac{1}{c^2}\frac{\partial^2}{\partial t^2}\right]\vec{A}(\vec{r},t) = -\frac{4\pi}{c}\vec{J}_\perp(\vec{r},t) \,. \qquad (2.31)$$

The vector potential for a circularly-polarized plane wave propagating in the $\hat{z}$ direction is given by $\vec{A} = (1/k)\,E(z,t)[\sin(\psi),\cos(\psi),0]$, where $\psi = (kz - \omega t + \phi(z,t))$ and $\omega = kc$ is the angular frequency of the optical field. The operator, $\vec{\nabla}^2$, may be separated into transverse and longitudinal components, $\vec{\nabla}^2 = \vec{\nabla}_\perp^2 + \vec{\nabla}_z^2$. For initial development only perfect injection and plane wave propagation will be used, for which $\vec{\nabla}^2 = \nabla_z^2$ applies. It is assumed that the optical field envelope evolves slowly over time with respect to the optical period and varies slowly over space with respect to the optical wavelength. This is called the slowly-varying amplitude and phase approximation and is summarized by

$$\frac{\partial E}{\partial t} \ll \omega E \quad , \quad \frac{\partial \phi}{\partial t} \ll \omega \phi \quad ,$$

$$\frac{\partial E}{\partial z} \ll kE \quad , \quad \frac{\partial \phi}{\partial z} \ll k\phi \qquad (2.32)$$

16

To solve Eq. 2.31, each component of the left-hand side is evaluated. The results and the right-hand side are projected onto perpendicular vectors which will allow separation of the solution to Eq. 2.31 into two separate, but dependent equations. The first step is to take the second partial derivative of $\vec{A}$ with respect to z which results in

$$\frac{\partial^2 \vec{A}}{\partial z^2} = \left[\frac{1}{k} \frac{\partial^2 E}{\partial z^2} - \frac{E}{k} \left(k + \frac{\partial \phi}{\partial z} \right)^2 \right] [\sin(\psi), \cos(\psi), 0]$$

$$+ \left[\frac{2}{k} \left(k + \frac{\partial \phi}{\partial z} \right) \frac{\partial E}{\partial z} + \frac{E}{k} \frac{\partial^2 \phi}{\partial z^2} \right] [\cos(\psi), -\sin(\psi), 0] \ .$$

(2.33)

Next, the second partial derivative of $\vec{A}$ with respect to t is divided by c^2 to get

$$\frac{1}{c^2} \frac{\partial \vec{A}}{\partial t} = \left[\frac{1}{c^2 k} \frac{\partial^2 E}{\partial t^2} - \frac{E}{kc^2} \left(\frac{\partial \phi}{\partial t} - \omega \right)^2 \right] [\sin(\psi), \cos(\psi), 0]$$

$$+ \left[\frac{2}{c^2 k} \frac{\partial E}{\partial t} \left(\frac{\partial \phi}{\partial t} - \omega \right) + \frac{E}{c^2 k} \frac{\partial^2 \phi}{\partial t^2} \right] [\cos(\psi), -\sin(\psi), 0] \ .$$

(2.34)

Adding Eq. 2.33 and Eq. 2.34 together and applying Eq. 2.32, results in all of the second-order terms dropping out and the resulting equations reduce to

$$\left[\nabla^{2z} - \frac{1}{c^2} \frac{\partial^2}{\partial t^2} \right] \vec{A} \approx -2E \left[\frac{\partial \phi}{\partial z} - \frac{1}{c} \frac{\partial \phi}{\partial t} \right] [\sin(\psi), \cos(\psi), 0]$$

$$+ 2 \left[\frac{\partial E}{\partial z} + \frac{1}{c} \frac{\partial E}{\partial t} \right] [\cos(\psi), -\sin(\psi), 0] \ .$$

(2.35)

If two unit vectors are defined by $\hat{\varepsilon}_1 = [\cos(\psi), -\sin(\psi), 0]$ and $\hat{\varepsilon}_2 = [\sin(\psi), \cos(\psi), 0]$, Eq. 2.35 is combined with the right-hand side of Eq. 2.31, and the dot products of $\hat{\varepsilon}_1$ and $\hat{\varepsilon}_2$ are found for both sides of the resulting equation, then the result is

17

$$\left[\frac{\partial E}{\partial z} + \frac{1}{c}\frac{\partial E}{\partial t}\right] = -\frac{2\pi}{c}\vec{J}_\perp \cdot \hat{\varepsilon}_1 \,,$$

$$E\left[\frac{\partial \phi}{\partial z} - \frac{1}{c}\frac{\partial \phi}{\partial t}\right] = \frac{2\pi}{c}\vec{J}_\perp \cdot \hat{\varepsilon}_2 \,.$$

(2.36)

The current density $\vec{J}_\perp$ is composed of the sum of the individual electron currents. Combining this sum with $\beta_\perp$ from Eq. 2.21, the right hand sides of Eq. 2.36 become

$$\vec{J}_\perp \cdot \hat{\varepsilon}_1 = \frac{ecK}{\gamma}\sum_i \cos(\psi + k_0 z_i)\delta^{(3)}(\vec{r} - \vec{r}_i)$$

$$\vec{J}_\perp \cdot \hat{\varepsilon}_2 = \frac{ecK}{\gamma}\sum_i \sin(\psi + k_0 z_i)\delta^{(3)}(\vec{r} - \vec{r}_i)$$

(2.37)

where $\vec{r}_i$ is the position of the ith electron. To get a useful approximation for the current density, an average over all of the electrons weighted by the number density of the electrons in the electron beam ρ is used. If it is assumed that a long electron pulse relative to the wavelength of the light is used and that there are no optical modes along the length of the undulator, then the approximations $\partial E/\partial z \rightarrow 0$ and $\partial \phi/\partial z \rightarrow 0$ can be made. These approximations and the averaging of $\vec{J}_\perp$, along with the definitions of ψ and τ, are used to find

$$\frac{\partial E}{\partial \tau} = -\frac{2\pi eK\rho L}{\gamma}<\cos(\zeta + \phi)>$$

$$E\frac{\partial \phi}{\partial \tau} = \frac{2\pi eK\rho L}{\gamma}<\sin(\zeta + \phi)>$$

(2.38)

which together, are the real and imaginary parts of

$$\frac{\partial}{\partial \tau}Ee^{i\phi} = -\frac{2\pi eKL\rho}{\gamma}<e^{-i\zeta}> \,.$$ (2.39)

If a, the dimensionless complex optical field strength, and j, the dimensionless current density, are defined by

18

$$a \equiv \frac{4\pi NeKLEe^{i\zeta}}{\gamma^2 mc^2}$$

(2.40)

$$j \equiv \frac{8N(e\pi KL)^2 \rho}{\gamma^3 mc^2} \ ,$$

then Eq. 2.38 can be rewritten as

$$\overset{\circ}{a} = -j <e^{-i\zeta}> \ ,$$

(2.41)

which is known as the dimensionless FEL wave equation and describes the evolution of the optical wave as it propagates along the undulator in phase space. The results are similar for a linear undulator [4], where the FEL parameter K is replaced by $K(J_0(\xi) - J_1(\xi))$ and E is replaced by $\bar{E} = E/\sqrt{2}$ in the terms a and j in the preceding derivation. For typical FELs, the efficiency is low, on the order of 10%.

F. ELECTRON BEAM QUALITY

For electrons not injected perfectly, the focusing of the electrons back towards the axis produces betatron oscillations [4]. The harmonic betatron oscillations have a constant of motion [4], $H_\beta = [\omega_\beta^2 y^2(\tau) + \overset{\circ}{y}{}^2(\tau)]/2 = [\omega_\beta^2 y_0^2 + \overset{\circ}{y}{}^2(0)]/2$ where y_0 is the initial electron transverse position, $\overset{\circ}{y}(0) = L\theta_y$, and θ_y is the initial injection angle. An electron injected off-axis at y_0 or at an angle of θ_y will experience an average phase velocity change of

$$\Delta \bar{v} \approx \frac{-kH_\beta}{L} = -\frac{2\pi N}{1+K^2}(K^2 k_0^2 y_0^2 + \gamma^2 \theta_y^2) \ .$$

(2.42)

For $|\Delta \bar{v}_\beta| \gtrsim \pi$, the gain bandwidth, the FEL's ability to bunch the electrons and produce gain will become inhibited.

The measure of the ability of an electron accelerator to inject electrons into an FEL with the proper initial position and velocity is called emittance, $\varepsilon_y = \bar{y}_0 \bar{\theta}_0$ for a linear undulator and $\varepsilon = \bar{r}_b \bar{\theta}_0$ for a helical undulator where $\bar{y}_0$ and $\bar{r}_b$ are the rms initial positions and $\bar{\theta}_0$ is the rms initial angular deflection of the electrons away from the z

19

axis. For any accelerator, either $\bar{y}_0$ or $\bar{\theta}_0$ may be reduced by external focusing, but the product ε is fixed. In order to minimize $\Delta\bar{v}$ in Eq. 2.42, the angular and position spreads are matched so that $Kk_0\bar{y}_0 = \gamma\bar{\theta}_y$. For a beam with matched emittances, Eq. 2.42, and the resonance condition, Eq. 2.18, can be used to show that $\Delta\bar{v}_\beta \approx 2\pi NKk\varepsilon_y/\gamma$. Since it is required that $|\Delta\bar{v}_\beta| \lesssim \pi$ in order to maintain proper FEL coupling, then $\varepsilon_y^{max} \approx \gamma/NKk = \gamma\lambda/2\pi NK$. Typical FEL's require a maximum emittance of ≈ 1 mm-mradian. With this limitation on electron beam quality, the effectiveness of the FEL at producing coherent light is dependent on several design parameters. These parameters are more restrictive when the optical wavelength, λ, is short or when the number of undulator periods, N, is large.

Inadequate beam quality can degrade FEL performance by inhibiting electron bunching. For the studies on SELENE, the electron beam is considered to be injected into the oscillator with initial electron energies distributed about v_0 in a Gaussian distribution with standard deviation of $\sigma_G = 4\pi N \overline{\Delta\gamma}/\gamma$. The injection angle is assumed to be an exponential distribution centered at zero with a standard deviation of $\sigma_\theta = 4\pi N\gamma^2\bar{\theta}^2/(1+K^2)$.

G. PHASE-SPACE AND THE LOW CURRENT, LOW GAIN FEL

Since the pendulum equation is periodic within an optical wavelength, the evolution of the electron with respect to its phase and phase velocity relative to the optical field over a distance of one wavelength of light can be studied in order to determine the overall characteristics of the FEL. Figure 2 shows the evolution of the electrons as they traverse the undulator. The electrons are initially injected into the undulator on resonance, $v_0 = 0$. From Eq. 2.23, electrons, whose phase with respect to the optical field is $-\pi/2 < \zeta < \pi/2$, will accept energy from the optical field. These electrons are depicted on the left side of the v versus ζ, or phase-space, plot. The electrons are shaded so that at the beginning of the undulator they are a light grey, and become darker as they travel down the undulator. Thus, as the electrons on the

left-hand side of the phase-space plot travel down the undulator, they gain energy. This increases their phase velocity and they begin to advance in phase with respect to the optical field. For the electrons on the right-hand side of the phase space plot, $\pi/2 < \zeta < 3\pi/2$. They lose energy to the optical field as they propagate down the undulator. Due to this decrease in energy, their phase velocity is reduced and they retard in phase with respect to the optical field. These effects combine to produce the clockwise rotational effect in the phase space plot.
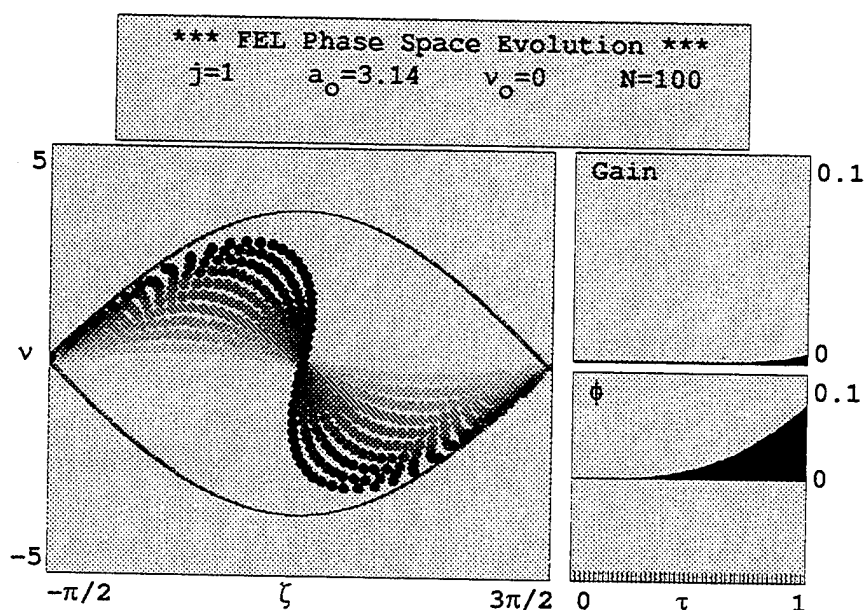

Figure 2. Phase-Space plot for an electron beam injected at resonance.

This clockwise rotation can be understood by looking at the pendulum equation, Eq. 2.28, and comparing it to a mechanical pendulum. Each electron is injected into the undulator with an initial position in phase space, (ζ_0, v_0). The points $(-\pi/2, 0)$ and $(3\pi/2, 0)$ are unstable fixed points. This is similar to the mechanical pendulum being at the top of its arc. The position $(\pi/2, 0)$ is a stable fixed point and it represents the mechanical pendulum being at the bottom of it's arc. The separatrix, represented on the phase space plot by a solid line, shows the boundary between open and closed

orbits for the electrons. The open orbits represent a mechanical pendulum with enough total energy to rotate through the unstable fixed points. The equation for the separatrix is given by [4]

$$v_s^2 = 2\,|a|\,[1-\sin(\zeta_s + \phi)]\,,\qquad(2.43)$$

which results in a total height of $4|a|^{1/2}$. From this, two important facts with regards to closed orbits can be seen. First, as the optical field strength grows, the maximum height of the separatrix grows. Also, since the equation for the separatrix depends on the combined electron phase, ζ and the optical phase ϕ, the separatrix will shift in ζ as the phase of the optical wave evolves in the undulator. This will typically happen with large current densities, $j > \pi$ and strong optical fields, $|a| > \pi$.

In Fig. 2, the electron beam was considered monoenergetic, and thus, all of the electrons are injected into the undulator with the same phase velocity, $v_0 = 0$. However, since the electron beam has a finite length much greater than the optical wavelength with a relatively large number density of electrons in the beam, it is considered that the electrons are injected with random phases with respect to the optical wave. In the phase space plots used, the phases were equally distributed between $-\pi/2$ to $3\pi/2$. From this and Fig. 2, it is seen that the same number of electrons will lose energy as gain, thus the overall energy transfer from the electrons to the optical field is zero.

In Fig. 2, to the right of the phase-space plot are two plots. The top one is a plot of the gain experienced by the optical field as it propagates down the undulator. The bottom one shows the evolution of the phase of the optical wave as it interacts with the electron beam in the undulator. The gain is defined as a function of τ and v_0 by

$$G(v_0,\tau) \equiv \frac{a(\tau)^2 - a_0^2}{a_0^2}\,,\qquad(2.44)$$

representing the fractional increase in the power contained in the optical field, where a_0 is the initial optical field at $\tau = 0$. For low current FELs, the average energy lost by

one electron to the optical field is $\gamma mc^2(<v>-v_0)/4\pi N)$ where $<v>$ is the average phase velocity of the electrons at τ. In weak optical fields the gain is [4]

$$G(v_0,\tau) = j\left[\frac{2-2\cos(v_0\tau)-v_0\tau\sin(v_o\tau)}{v_0^3}\right],$$ (2.45)

where v_0 is the initial phase velocity of the incident electron beam.

The bottom plot on the right-hand side of Fig. 2 represents the evolution of the optical field phase, ϕ, as a function of τ. From Eq. 2.23 $\dot{\gamma}/\gamma \approx 0$ for electrons near $\zeta+\phi = \pi/2$,and there is little energy transferred between the optical field and the electrons. However, the interaction between the electrons and the optical field results in the phase of the optical field changing as shown in Equations 2.40 and 2.41. This optical phase shift affects the phase relationship between the electrons and the optical field as will be shown in the case of strong optical fields.

Figure 3 is a graph of $G(v_0)$ at $\tau = 1$ for low current, $j = 1$, and weak field, $a_0 < \pi$, conditions with perfect beam injection. This clearly shows that as the initial phase velocity increases above resonance, more energy is
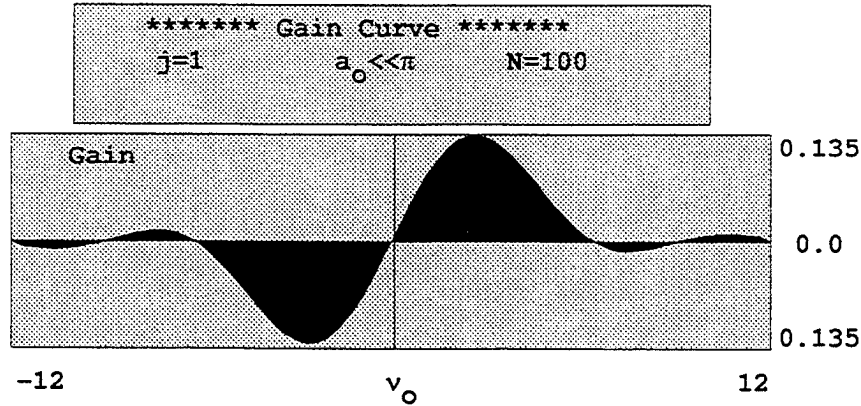

Figure 3. Gain spectrum for a low current, weak field FEL.

transferred to the optical field. However, if the initial phase velocity is too high, then a larger fraction of the electrons are no longer in closed orbits and will not couple with

23

the optical field. This results in a degradation in the gain as v_0 increases. Maximizing $G(v_0, \tau)$ with respect to v_0 results in $G = 0.135j$ at $v_0 = 2.6$. Note that since $G(v_0, \tau)$ is proportional to j, the terms low gain, and low current are interchangeable.

In Fig. 4, the electron beam is injected into the undulator off-resonance at $v_0 = 2.6$ where the gain is a maximum. This corresponds to a higher average energy in the electron beam than in Fig. 2, and more energy will be transferred to the optical field by the electrons than will be absorbed. Note that some of the electrons near the edges of the phase space plot will have open orbit trajectories, while those electrons within the separatrix will have closed orbits. The electrons in closed orbits begin to "bunch" near $\zeta = \pi$. From the wave equation, Eq. 2.41, it can be seen that bunching at this phase will drive the optical field amplitude and produce gain. As the number of electrons with the same relative phase increases, the radiation from the electrons becomes coherent.
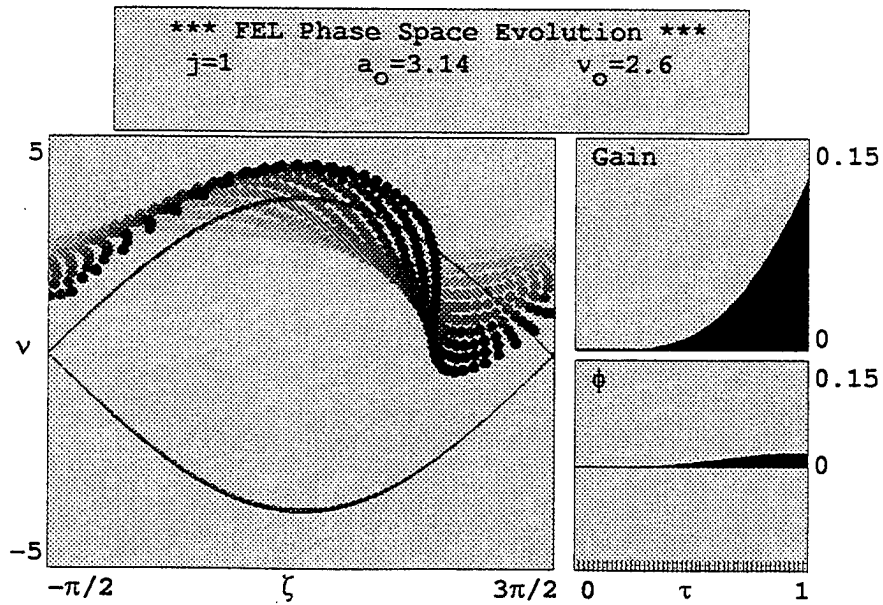

Figure 4. Phase-Space plot for an electron beam injected at $v_0 = 2.6$.

In order to understand the interaction between the electron beam and the optical field, the pendulum equation must first be revisited. Using the definitions $v = \overset{\circ}{\zeta}$ and $\zeta = (k+k_0)z - \omega t$, and assuming weak fields and low gain, the pendulum equation can be expanded to get an electron's phase and phase velocity with respect to the optical wave as a function of τ,

$$\zeta(\tau) = \zeta_0 + v_0\tau - \frac{a_0}{v_0^2}[\cos(\zeta_0 + v_0\tau) - \cos(\zeta_0 + v_0\tau)\sin(\zeta_0)] + ..., \tag{2.46}$$

and

$$v(\tau) = v_0 + \frac{a_0}{v_0}\left[\sin(\zeta_0 + v_0\tau) - \sin(\zeta_0)\right] +$$

$$\tag{2.47}$$

$$\frac{a_0^2}{v_0^3}\left[-\frac{1}{4}[\cos(2\zeta_0 + 2v_0\tau) - \cos(2\zeta_0)] + \cos(v_0\tau) - 1 - v_0\tau\sin(\zeta_0)\cos(\zeta_0 + v_0\tau)\right] + ...$$

Using Eq. 2.46 and Eq. 2.47, Eq. 2.41 can be solved for the optical field strength and phase evolution as a function of τ,

$$|a(\tau)| = a_0\left[1 + j\left[\frac{2 - 2\cos(v_0\tau) - v_0\tau\sin(v_0\tau)}{2v_0^3}\right] + \cdots\right], \tag{2.48}$$

and

$$\phi(\tau) = j\left[\frac{2\sin(v_0\tau) - v_0\tau(1 + \cos(v_0\tau))}{2v_0^3}\right] + \cdots . \tag{2.49}$$

For electrons injected with a phase velocity $v_0 \approx \pi$, as in Fig. 4, Eq. 2.48 shows that the optical field is amplified at $\tau = 1$. With electrons injected at $v_0 \approx -\pi$, the optical field is not amplified and, in fact, begins to lose energy to the electrons as they bunch near $\zeta = 0$. When the electrons are injected on resonance, $v_0 = 0$, at low current and weak fields, as in Fig. 2, the electrons bunch near $\zeta = \pi/2$. This results in very little gain in the optical field as shown by Eq. 2.48, however, Eq. 2.49 shows that the optical phase is advanced. With this information, and Fig. 4, the range of v_0 for good coupling between the electron beam and the optical field is found to be in the range of $|v_0| \lesssim \pi$.

The FEL natural gain bandwidth can be found from $\Delta v_0 \approx 4\pi N \Delta \gamma / \gamma$ and is given by

$$\left| \frac{\Delta \gamma}{\gamma} \right| \approx \frac{1}{2N} \, . \tag{2.50}$$

H. HIGH CURRENT, HIGH GAIN FELS

In the previous discussion, low currents, $j \lesssim 1$, and weak fields, $|a_0| \lesssim \pi$, were assumed in order to derive analytical approximations which describe the evolution of the electrons and the optical field as a function of τ. However, if $j \gg 1$, these assumptions are no longer valid and in order to study the FEL in these conditions, the pendulum and wave equations must be used as a starting point. The basic principle of the FEL does not change. The gain still depends on the ability of the FEL to bunch electrons and produce coherent radiation.

Figure 5 is a phase space plot of an FEL with a dimensionless current density of $j = 100$, a relatively weak field of $a_0 = \pi$, no spread in phase velocity, and uniform phase distribution. The initial phase velocity of $v_0 = 1.8$ is the phase velocity at which maximum gain is achieved for this FEL. At the beginning of the undulator, near $\tau = 0$, the electrons begin to bunch near $\zeta + \phi = \pi/2$. During this initial interaction time, there is no gain in the optical field, or change in the optical phase, as can be seen by the gain and phase plots on the right in Fig. 5. Since the electrons are near resonance, they begin to drive the optical phase instead of the optical field which shifts the separatrix to the left. As the optical phase shifts, the combined phase $\zeta + \phi$ begins to shift towards π, and the optical field is amplified. At $\tau \approx 0.5$, the gain grows exponentially and continues to the end of the undulator. The strong shift in phase of the optical field shifts the separatrix to the left by $\approx \pi/2$ and the electrons bunch near $\zeta = \pi/2$, or $\zeta + \phi \approx \pi$ for optimum gain.

The analytical solution for the high current case may be derived from Eq. 2.28 and Eq 2.41 by using perturbation methods and integrating over all initial phases [4].
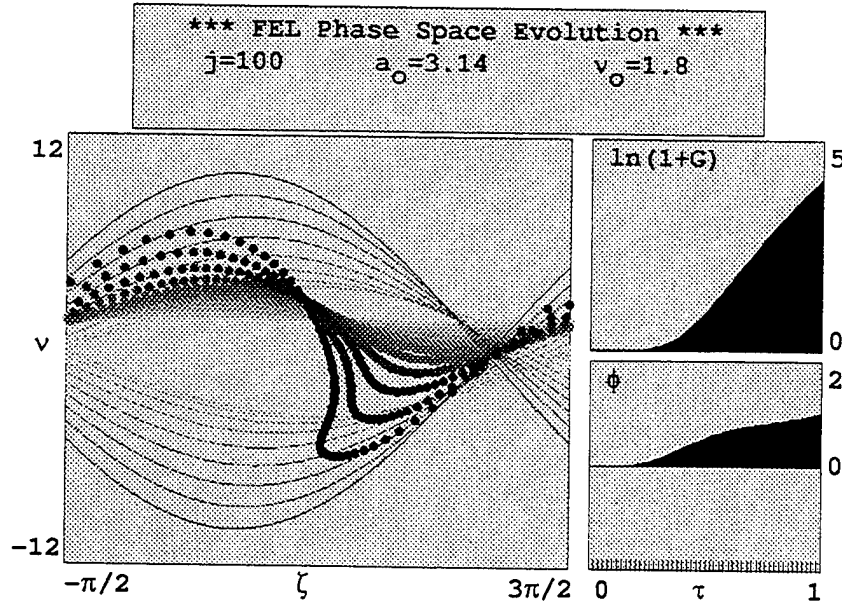
Figure 5. Phase-Space plot for a high current FEL.

In doing so, it is found that for small times, $\tau \ll 1$, $a(\tau) = a_0(1 + ij\tau^3/12 + \cdots)$ and there is little gain in the optical field. The optical phase, however, increases slowly and in proportion to τ^3. For $\tau \lesssim (2/j)^{1/3}$, the electrons are bunching. As soon as bunching is sufficient to produce coherent stimulation, the high current causes exponential growth in the optical field strength. For high current, $j \gg 1$, the optical field strength, phase, and gain are given by

$$|a(\tau)| \approx \frac{a_0}{3} e^{(j/2)^{1/3}\sqrt{3}\tau/2} ,$$
(2.51)

$$\phi(\tau) \approx (j/2)^{1/3}\tau/2 ,$$
(2.52)

and

$$G(\tau) = \frac{1}{9} e^{(j/2)^{1/3}\sqrt{3}\tau} .$$
(2.53)

Figure 6 shows the high gain spectrum for $j = 100$ and $a_0 = 1$. The gain spectrum is no longer antisymmetric about $v_0 = 0$, instead it is nearly symmetric about

27

the phase velocity which produces the maximum gain. This is true in general for high current FELs. The peak gain occurs for a phase velocity that is closer to resonance than in the low current case. Gain continues to be positive even for negative values of v_0 near resonance. The gain spectrum bandwidth at which $G(v_0) = 1/e\ G_{max}$, is $\Delta v_0 \approx 4j^{1/6} \approx 2\pi$ and is much wider than that for the low current FEL.

****** Gain Curves ******
j=100 a_o=1

Gain	71
	0.0
	-71

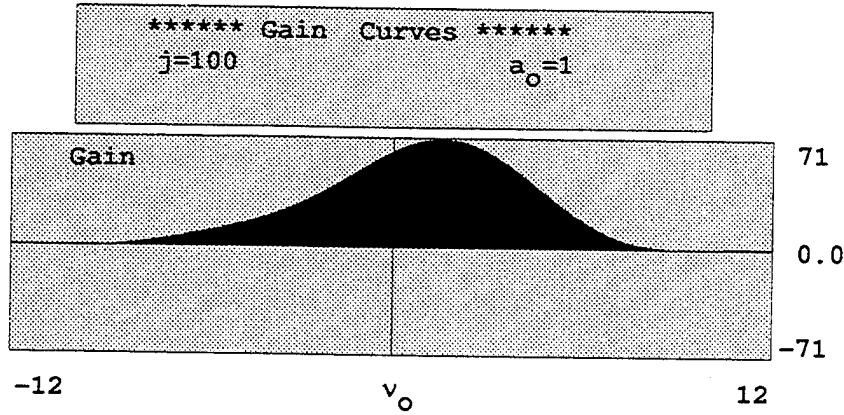-12 v_o 12

Figure 6. Gain spectrum for a high current FEL .

The characteristic energy spread at which gain degradation begins no longer follows that of the low current FEL of $\sigma_G < \pi$. The FEL becomes more resistant to gain degradation when the optical field amplitude grows exponentially. From Eq. 2.53 it can be seen that for high current FELs, the growth rate is exponential for strong fields. The characteristic energy spread at which gain degradation begins is comparable to this growth rate, $\sigma_G \approx j^{1/3}$ [4].

I. SATURATION IN STRONG OPTICAL FIELDS

So far, only weak optical fields have been considered. Equations 2.28 and 2.41 are both valid for all cases of strong and weak fields as well as low and high current FELs. Using the phase-space plots will help in understanding the interactions associated with strong optical fields and the electron beam. Figure 7 is a phase-space

plot for a low current, $j = 1$, FEL with initial optical field strength of $a_0 = 20$. The electron bunching seen in Fig. 4 has been extended until the condition of overbunching is reached. The electrons began to bunch at $\zeta + \phi = \pi$. As they continue down the undulator, they transfer more energy to the optical field until they have transferred the maximum amount of energy to the optical field. At this point, they begin to absorb energy from the optical field. This is called overbunching and is indicated by a reduction in the gain. The gain plot of Fig. 7 shows the initial rise in gain due to the strong optical field, and at $\tau \approx 1/2$, maximum bunching occurs as indicated by the maximum rate of change in gain. At $\tau \approx 0.8$, the electrons have transferred all of their available energy to the optical field and begin absorption. The final gain of 0.03 is significantly reduced from that of 0.135 in Fig. 4. This reduction in gain in the presence of strong optical fields is expected for two reasons. In order to achieve the same gain with a larger initial optical field strength, the amount of energy transferred to the optical field must also be proportionally larger. The overbunching of the electrons inhibits the ability of the electron beam to transfer energy to the optical field. The evolution to an overbunching condition necessarily requires that the electrons pass through the condition where they are bunched at $\zeta + \phi = \pi/2$ where they will advance the phase of the optical field. This can be seen in Fig. 7 where the optical phase shift increases near $\tau \approx 0.5$. This particular case does not result in a significant phase shift in the optical field, $\phi < 0.003$, since the electron current is low.

Figure 8 is a phase-space plot of an FEL with high current and strong optical fields. The overbuncing is noticeable. The optical phase also advances more than in the low current case. This shifts the separatrix to the left. The overall gain is, as expected, significantly less than for the weak field case of Fig. 5.

The evolution to saturation in an FEL oscillator from weak fields is accompanied by a change in the optical frequency. In an oscillator, the semi-transparent mirror that allows the laser light to leave the oscillator cavity results in a reduction in the optical field strength. This loss, combined with other losses in the oscillator is quantified by

*** FEL Phase Space Evolution ***
j=1   a$_0$=20   v$_0$=5.8

12

ln(1+G)   0.03

v   0

φ   0.005

0

-12

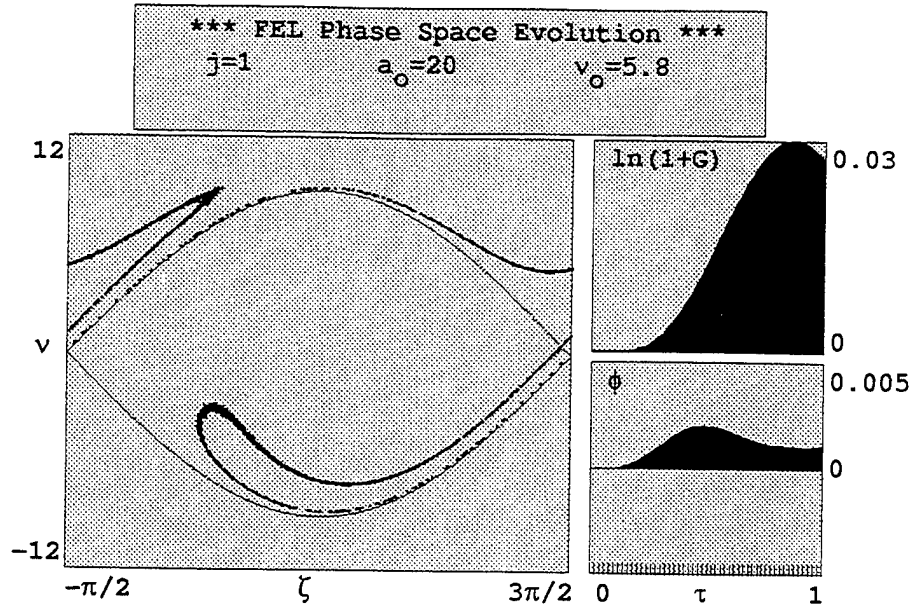$-\pi/2$ ζ $3\pi/2$ 0   τ   1

Figure 7. Phase-Space plot for a low current, strong field FEL.

the resonator Q factor defined in such a way that in the absence of an electron beam, the optical field is reduced by a factor of $e^{-1/Q}$ each pass. If the gain produced by the electron beam is sufficient to make up for these losses, then the optical field will grow. In weak fields, mode competition results in the optical frequency being centered around the frequency corresponding to $v_0 = 2.6$. As the optical field grows, the phase velocity for maximum gain shifts to the right and the optical wavelength decreases. In weak optical fields, with low Q, the FEL gain may not be sufficient to overcome the losses and the steady state optical field is zero. For larger values of Q, the FEL gain is sufficient to overcome the losses and the optical field grows. When the optical field reaches the point where saturation occurs during each pass, then the gain is reduced due to this saturation. As the gain falls off, the optical field continues to grow until the gain is insufficient to make up for the losses in the cavity and the growth rate of the optical field is reduced. The combination of saturation, cavity losses and gain
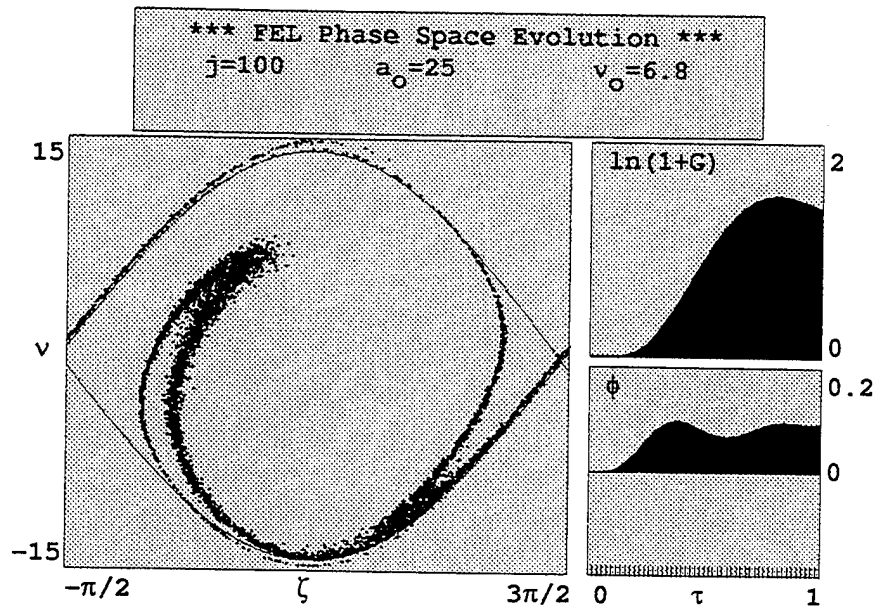
Figure 8. Phase-Space plot for a high current, strong field FEL.

work together to bring the FEL into steady state operation. This typically takes several hundred passes. This concept is important in the study of SELENE.

J. OPTICAL KLYSTRON FELS

One of the beneficial features of the FEL is the ability to change the characteristic output of the FEL by changing the undulator design. Several undulator designs are used for altering the interaction between the electron beam and the optical field. One of these designs shown in Fig. 9 is the optical klystron. The optical klystron is used to provide increased gain in weak fields. This is accompanied by saturation at lower optical field strengths compared to the standard FEL. The optical klystron consists of an FEL oscillator constructed with a dispersive or drift section, positioned at $\tau = 0.5$, between two undulator sections .

The first undulator section, or modulator, is used to prepare the electrons for bunching. When the electrons enter the dispersive section, the interaction with the
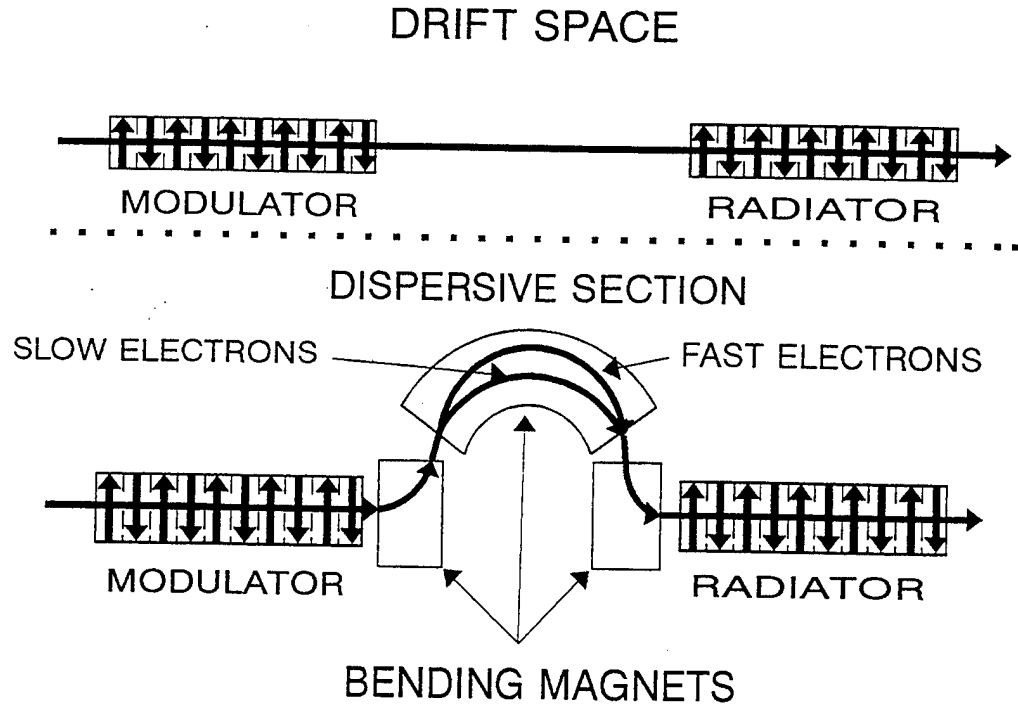
31

DRIFT SPACE

Figure 9. Optical klystron configurations.

optical field stops. In the *drift space*, this happens because the electrons are far from resonance, while in the *dispersive section* the electrons are bent out of the optical field by a large magnetic field. In the dispersive section, the electrons are bunched due to the differences in phase velocities between the electrons. The electrons with phase velocities greater than the average experience a larger Lorentz force than the slower electrons. As they pass through the magnetic field, they have a longer path length to travel before reentering the second undulator section. The opposite is true for the slower electrons. Thus, as the electrons enter into the second undulator section, or radiator, the electrons are bunched near the same phase relative to the optical field. With the electrons bunched prior to entering the second undulator segment, the ability of the electrons to radiate and transfer energy to the optical field is much greater.

Since the electrons do not interact with the optical field while they are in the dispersive section, they do not transfer energy to or from the optical field. However,

they do experience a phase shift that is directly proportional to their phase velocity and the dispersive strength, $\Delta\zeta = \nu D$. D is the dispersive strength of the klystron given in equivalent undulator lengths, $D = N_d/N$, where N_d is the number of undulator periods that would produce the same bunching. The dispersive strength is governed by the strength of the magnetic fields in the dispersive section and the undulator parameter K. A dispersive strength of one is equivalent to having doubled the length of the undulator. Equations 2.28 and 2.41 are still valid throughout the length of the undulator for an optical klystron. For $jD \ll 1$ and in the limit of $D \to \infty$ and $\nu_0 \to 0$ with the product $D\nu_0$ fixed, the gain as a function of ν_0 is [7]

$$G(\nu_0) \approx \frac{jD}{4}\sin(\nu_0 D) ,\qquad\qquad (2.54)$$

with a peak gain of $jD/4$ at $\nu_0 = \pi/2D$. This is illustrated in Fig. 10.

****** Gain Curves ******
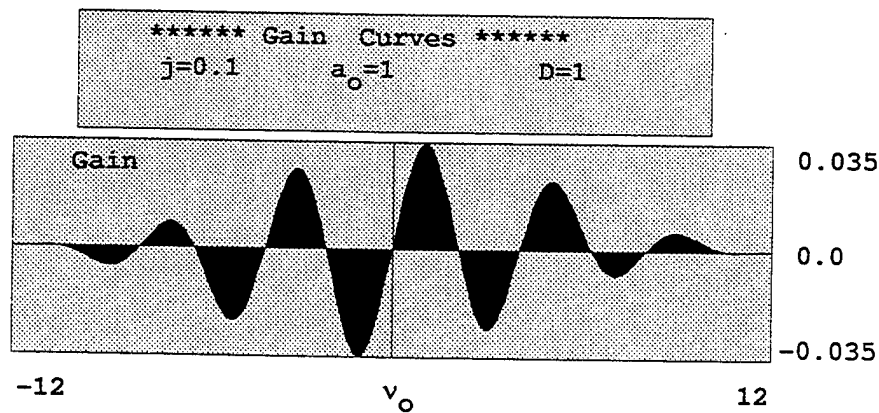j=0.1   a_o=1   D=1

Figure 10. Gain spectrum for a low current, weak field optical klystron FEL.

Figure 10 shows that there are several peaks in the region $|\nu_0| < 2\pi$. From Eq. 2.54, it is apparent that the electron beam quality should be such that $\Delta\nu_0 < \pi/D$ in order to maximize coupling and gain. Compared to the non-klystron FEL, where $\Delta\nu_0 < \pi$ is required, this is a significant restriction on using an optical klystron.

Figure 11 is a phase-space plot for an optical klystron in weak fields and low current. The electrons are injected into the undulator with uniform phase velocity of $v_0 = 1.1$ for maximum gain and are represented in light gray. As the electrons propagate down the undulator, they become darker until they reach the end of the undulator where they are shown in black. The evolution of the electrons in the modulator is similar to that of Fig. 4. The gain plot to the right of the phase-space plot shows that the optical field is not driven until after the dispersive section at $\tau = 0.5$. At this point, the electrons are given a step jump in phase, $\Delta\zeta = vD$, which can be seen in Fig. 11. This results in all of the electrons moving to the right a distance which is proportional to the phase velocity of the individual electrons. The electron beam and optical field interaction continues from this point to achieve the FEL output. The bunching is easy to see at $\zeta + \phi = \pi$ at the end of the second undulator. The final gain of 0.04 is almost three times that of the non-klystron undulator. This shows the usefulness of using the optical klystron configuration in FELs that have insufficient gain to startup.

In the presence of strong optical fields, the characteristics of the optical klystron changes dramatically. Figure 12 shows the gain spectrum for an optical klystron with $jD < 1$ and strong optical fields. Figure 13 is the phase-space plot for $v_0 = 4.1$ at which the maximum gain is achieved. The positions of the electrons in phase-space at $\tau = 0.5$, just prior to the dispersive section is plotted in light gray. The evidence of the strong optical fields is evident in that the electrons are already bunched prior to entering the dispersive section. When the electrons enter the dispersive section, the electrons are bunched at $\zeta + \phi = \pi$ and are all given a step displacement in ζ. Since they were previously bunched, this results in the electrons being dispersed instead of being bunched. This results in a reduction in gain by a factor of ≈ 7.5 as compared to the weak field case of Fig. 11. The electrons continue to interact with the optical field as they propagate down the radiator section and the final phase-space positions are plotted in dark gray in Fig. 13.
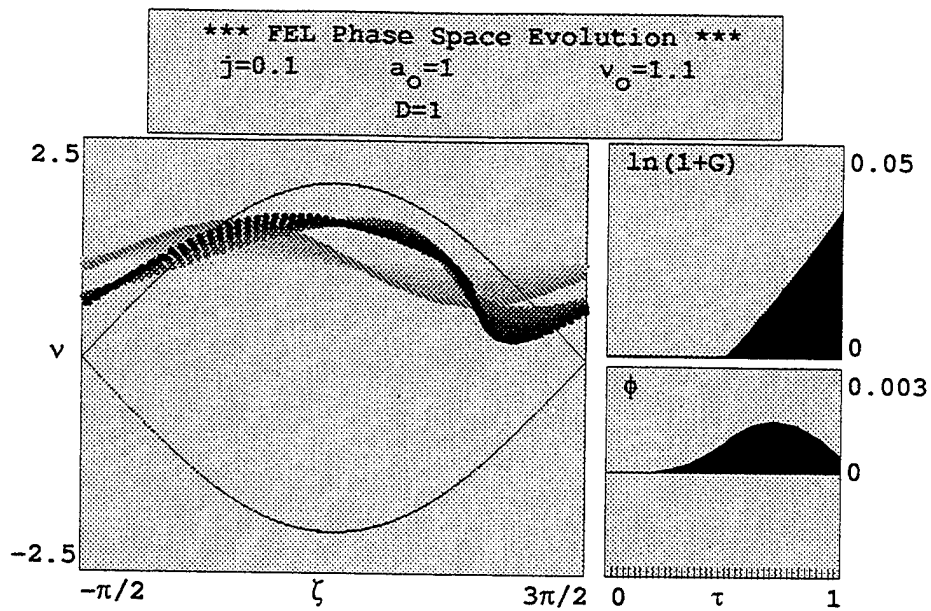
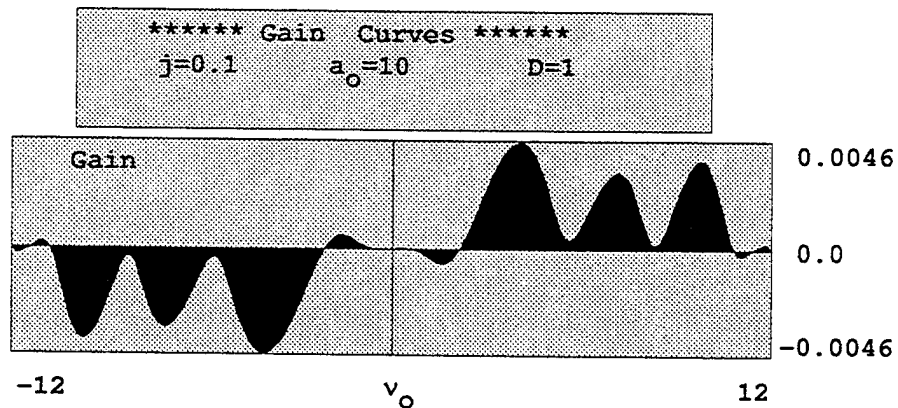Figure 11. Phase-Space plot for a low current, weak field optical klystron.

Figure 12. Gain spectrum for a low current, strong field optical klystron FEL.

In stronger optical fields, the modulator is efficient at bunching the electrons, so that when the electrons reach the dispersive section, the $\Delta\zeta$ induced by the dispersive section essentially redistributes the electrons evenly in phase with a large energy
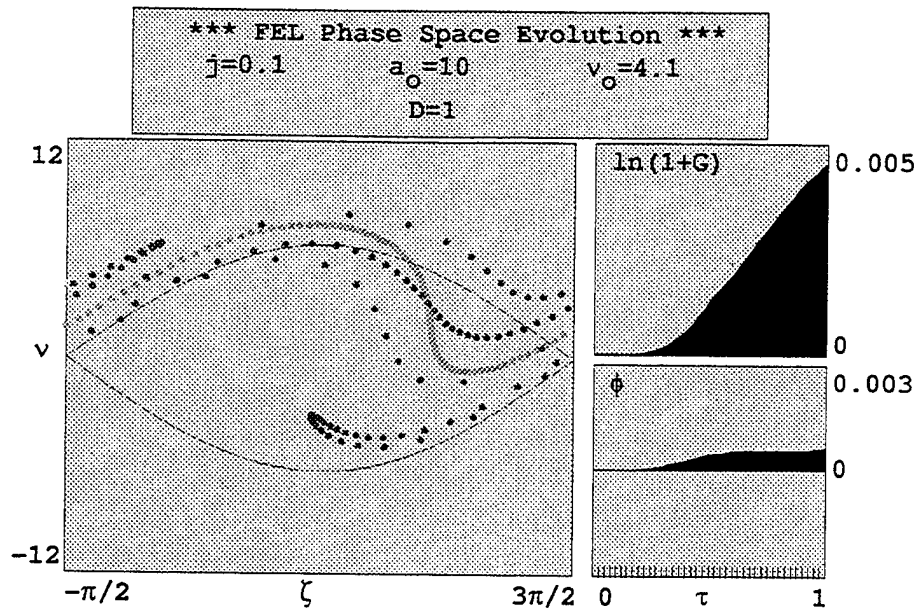
```
*** FEL Phase Space Evolution ***
j=0.1          a =10          v =4.1
                o              o
              D=1
```

Figure 13.   Phase-Space plot for a low current, strong field optical klystron FEL, $a_0 = 10$.

spread. This results in the electrons entering the radiator as a low quality electron beam instead of the highly bunched electron beam the dispersive section is designed to produce in weak fields.

The result of the dispersion effects of the optical klystron in strong optical fields is evident in Fig. 14, where, at $\tau = 0.5$, the gain flattens out until the electrons can be rebunched by the radiator section. The final gain from this FEL is significantly reduced to about half that of Fig. 13. This reduction in gain in the presence of strong optical fields is the reason why dispersive sections are designed to be used to produce high gain only in weak field FELs. This property of reduced gain in strong field optical klystron FELs can actually become an advantage, and will be exploited in the design of SELENE.
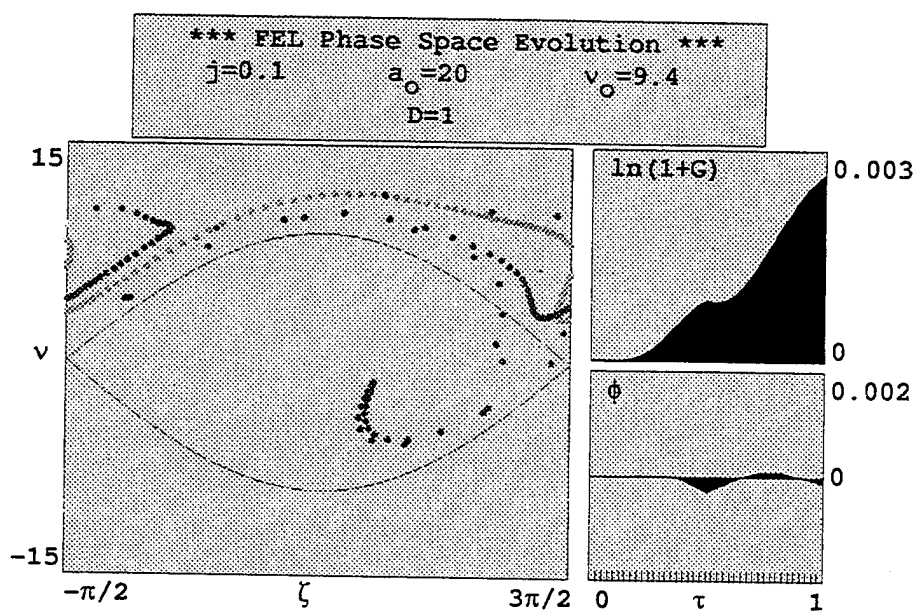
*** FEL Phase Space Evolution ***
$j=0.1$ $a_o=20$ $v_o=9.4$
$D=1$

Figure 14. Phase-Space plot for a low current, strong field optical klystron FEL, $a_0 = 20$.

III. SELENE AND NOVOSIBIRSK PROPOSALS

A. INTRODUCTION

As a joint venture, Russia and the United States are pursuing the development of a high power laser system to beam energy to satellites. The Budker Institute at Novosibirsk, Russia, is building a 200 kW system. The proposal for SELENE at China Lake, California, is intended to expand on this design to achieve a 10 MW system. Figure 15 is a schematic of the proposed system for SELENE. This consists of a three-section optical klystron oscillator followed by a radiator. The three undulator sections and the undulator in the radiator are identical. The electron beam will be provided by a 51 MeV racetrack microtron recuperator (RTMR) [9]. The oscillator is designed to bunch the electron beam prior to entering the radiator. The dispersive sections in the oscillator are designed to be variable in strength. The electron beam is bent out of the oscillator and sent to the radiator which uses coherent spontaneous emission from the bunched electron beam to generate a high power laser beam. This beam is transmitted along a two mile vacuum tube to allow it to expand by diffraction to reduce the incident laser intensity on the mirror. The beam is reflected off of an adaptive mirror either to the satellites directly, or to a beacon satellite which will then direct the laser to the proper satellites.

B. SIMULATION PARAMETERS

The electron beam is 20-100 ps in duration with a repetition frequency of 2 - 45 MHz. The peak current is 20 - 100 A. The emittance is estimated at 0.628 mm-mrad. The 51 MeV electrons have a Lorentz factor of $\gamma = 100$. The peak electron beam current of 100 A, and the beam area of $\pi r_b = 0.002 \text{cm}^2$, where r_b is the electron beam radius, results in an average filling factor of $\overline{F} = 0.18$ over the entire system and $\overline{F} = 0.23$ in the oscillator. The total dimensionless current density is the product of the
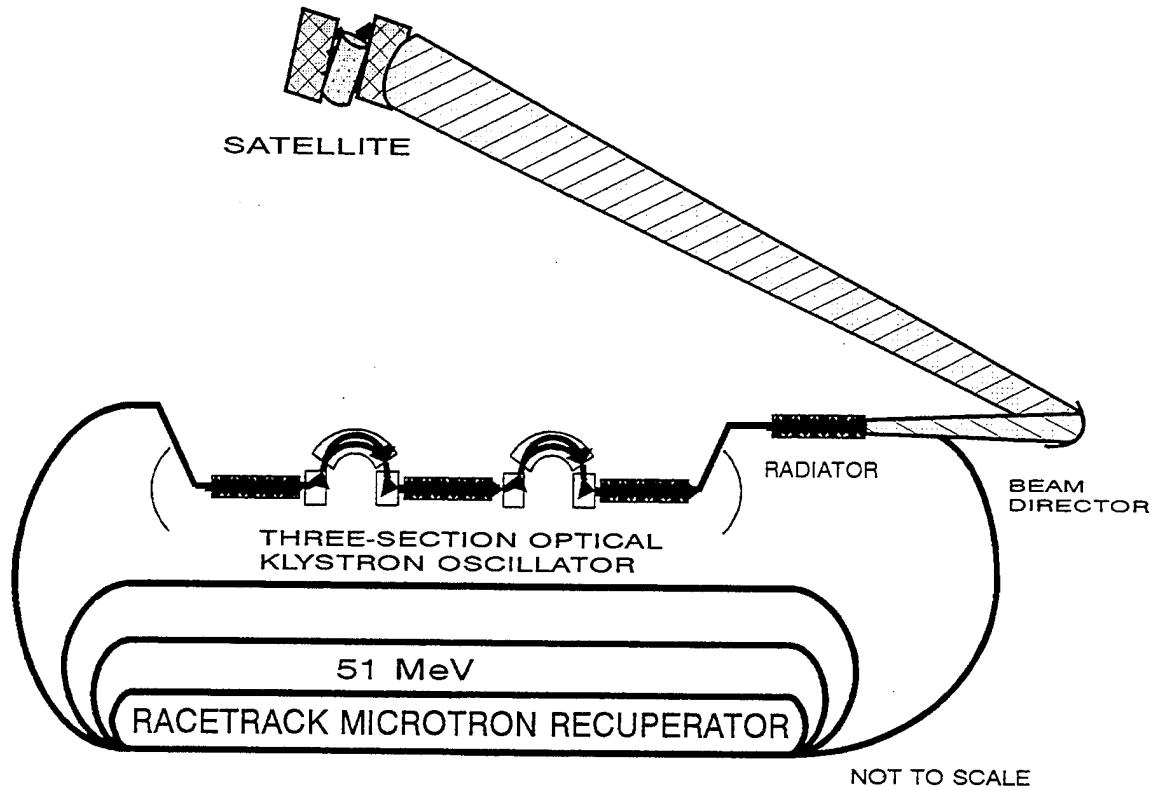
39

Figure 15. Schematic diagram of the SELENE FEL system.

dimensionless current density j and the filling factor $\bar{F}$. For further ease, the total dimensionless current density will be represented by $j\bar{F} \to j$. The parameters above result in a total dimensionless current of $j = 180$ for the entire system, and $j = 100$ for just the oscillator. The design energy spread is $\Delta\gamma/\gamma = 0.045\%$ which results in an initial phase velocity spread of $\Delta v = \sigma_G = 4\pi N\Delta\gamma/\gamma = 0.67$ for the oscillator and $\sigma_G = 0.9$ for the system as a whole. Assuming the electron beam has been groomed for matched angular and radial distributions, the rms angular deviation from the z axis is $\bar{\theta} = \varepsilon/\pi r_b = 0.00025$ and the angular spread is characterized by $\sigma_\theta = 0.32$.

Each undulator section consists of 40 undulator periods. Each period is 9 cm in length, for a total length of 3.6 m for each section. The proposed dispersive section strength is equivalent to $D = 0.5$ for each dispersive section in the oscillator. The

40

space between the oscillator and the radiator also acts like a dispersive section with an equivalent dispersive strength of $D_r = 0.25$. When the oscillator is studied as a separate unit, the dispersive strength for each dispersive section scales to $D = 0.67$. During the study of the oscillator it is desirable to compare the effects of this three-section oscillator to a two-section oscillator. For the three-section oscillator, the dispersive strength stated is for one of the dispersive sections. For the two-section oscillator used to compare with SELENE's oscillator, the dispersive strength of $D = 1.3$ will be used to closely approximate the total dispersive strength of both dispersive sections in the three-section klystron. The mirrors in the oscillator section are separated by a distance of 79 m. The FEL undulator parameter of $K = 1.4$ [9] corresponds to a optical wavelength of 13 μm and $\xi = 0.3$, where ξ is defined following EQ. 2.30.

C. OPTICAL DEVICE LIMITATIONS

A major concern in the SELENE FEL design is the durability of the mirrors in the oscillator. The beam from the radiator has a two mile propagation distance to spread out and reduce the laser intensity on the mirrors that project the laser to the satellites. The oscillator, on the other hand, has an 11 meter undulator section in a 79 meter oscillator cavity. The high electron beam current results in high gain and thus strong optical fields after saturation has occurred. Mirror construction is a highly specialized field and the materials used to construct them vary widely in their ability to withstand high intensity laser light. Mirrors are available to operate with peak intensities of $1\,\mathrm{GW/cm^2}$ with pulse lengths of 0.1 ns and a ten percent duty cycle [10]. Mirrors have been demonstrated which can withstand an average power density of $10\text{--}100\,\mathrm{kW/cm^2}$ with a continuous duty cycle [11]. In order to provide a safety margin, the maximum intensity allowed on the mirrors is assumed to be $50\,\mathrm{kW/cm^2} = 5 \times 10^{11}\ \mathrm{ergs/cm^2 s}$ for SELENE. If the Rayleigh length is matched to an individual undulator section, then $z_0 \approx 4$ meters. The expansion of the optical wave due to diffraction is given by

41

$$w^2 = w_0^2 \left[1 + \frac{S_m^2}{z_0^2} \right] , \tag{3.2}$$

where S_m is the mirror separation distance, w is the radius of the beam spot size at the mirrors, w_0 is the optical beam radius at the waist which is usually in the center of the undulator, and $z_0 \lambda = \pi w^2{}_0$. The magnitude of the optical field intensity at the mirrors is [12]

$$|\vec{S}| = |\vec{E}|^2 c/4\pi . \tag{3.3}$$

Thus the maximum allowable optical field strength in the undulator to prevent mirror damage is

$$|a| = \left[1 + \frac{S_m^2}{z_0^2} \right]^{1/2} \frac{4\pi NeK(J_0(\xi) - J_1(\xi))L}{\gamma^2 mc^2} \left[\frac{4\pi}{c} |\vec{S}| \right]^{1/2} . \tag{3.4}$$

Using the numbers presented above for this system, the maximum dimensionless optical field strength in the undulator is $|a| \approx 30$. This is well into the strong field regime. Once the optical field is reduced below this value for steady state operation, the concern is to ensure the oscillator is able to perform the function for which it was designed, that is, to provide a bunched electron beam to the radiator. As discussed previously, strong optical fields result in overbunching and thus this will inhibit the ability of the radiator to produce coherent spontaneous emission. The spontaneous emissions are required to establish an optical field for the electron beam to interact with in the single pass radiator.

Figures 13 and 14 demonstrate that strong optical fields are undesirable if the electrons are required to be bunched prior to entering the SELENE radiator. In strong optical fields, the electrons are bunched prior to entering the first dispersive section. When this happens, the dispersive section disperses the electrons instead of bunching them. It is important to remember that the electron beam for SELENE will encounter a third dispersive section prior to entering the radiator.

D. DISPERSIVE SECTION EFFECTS

The oscillator design of the SELENE system provides some challenging goals in trying to reduce the optical field strength sufficiently to prevent damage to the mirrors and to prevent destroying the bunching of the electrons prior to entering the radiator. Figure 16 shows the result of using optical klystrons in strong optical fields. This figure was produced using a series of gain spectra similar to Fig. 12 where the initial optical field strength was varied and the peak gain was recorded. In the weak field regime, $a_0 < \pi$, the dispersive sections increase the gain significantly. This will result in the optical field growing rapidly during each pass until the strong field condition is reached.
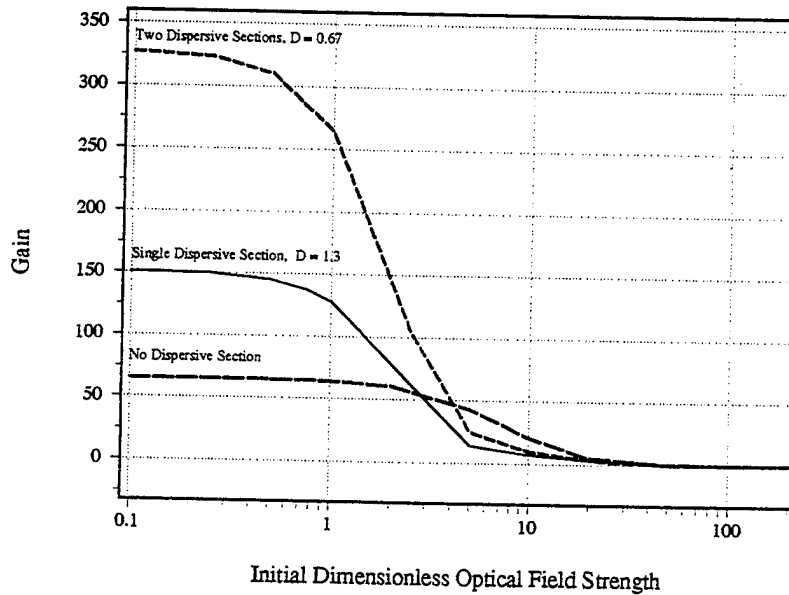

Figure 16.   Single pass maximum gain vs. dimensionless optical field strength for a three-section klystron, a two-section klystron, and a single undulator FEL oscillator.

Even though the two dispersive sections in the three-section klystron have the same total dispersive strength as the single dispersive section in the two-section

43

klystron, the three-section klystron produces more gain in weak fields than the two-section klystron. However, as the optical field strength increases, the gain in the three-section klystron oscillator becomes less than the gain for the two-section klystron. As the optical field continues to grow, the gain for the three-section klystron produces is reduced below that of the single undulator oscillator. Figure 16 is based on the single pass gain in an FEL with the same operating parameters as SELENE's oscillator.

Figure 17 is a plot of the single pass maximum gain as a function of the dispersive strength with an initial optical field strength of $a_0 = 10$. Three important features are visible in this plot. First, for both the three section and the two section klystrons, increasing the dispersive strength beyond $D = 2$ has little effect on the maximum gain of the system for $D \leq 4$. Next, it is evident that the three-section klystron has less gain at $a_0 = 10$ than the two section klystron for $D \geq 0.3$. This agrees with Fig. 16. The other major feature of note is the peak in gain at $D \approx 0.5$. The origin of Fig. 17 is a series of gain spectrum plots similar to Fig. 12. The maximum gain for each dispersive strength is plotted in Fig. 17. At $D \approx 0.5$ for both systems, the initial phase velocity giving the maximum gain shifts to a higher phase velocity.

Figure 18 shows this phenomenon in a form easier to interpret. If the phase velocity is kept constant and σ_G is small enough to ensure that few electrons are outside the central maximum shown in Fig. 18, then the gain will drop rapidly as the dispersive strength is increased. However, if the electron phase velocity is maintained at that velocity for which maximum gain is achieved, then the result is the effect shown in Fig. 17. The process of natural mode competition in the FEL oscillator maintains the relative phase velocities between the optical field and the electron beam so that the average phase velocity of the electron beam is that which produces the maximum gain in the optical field.
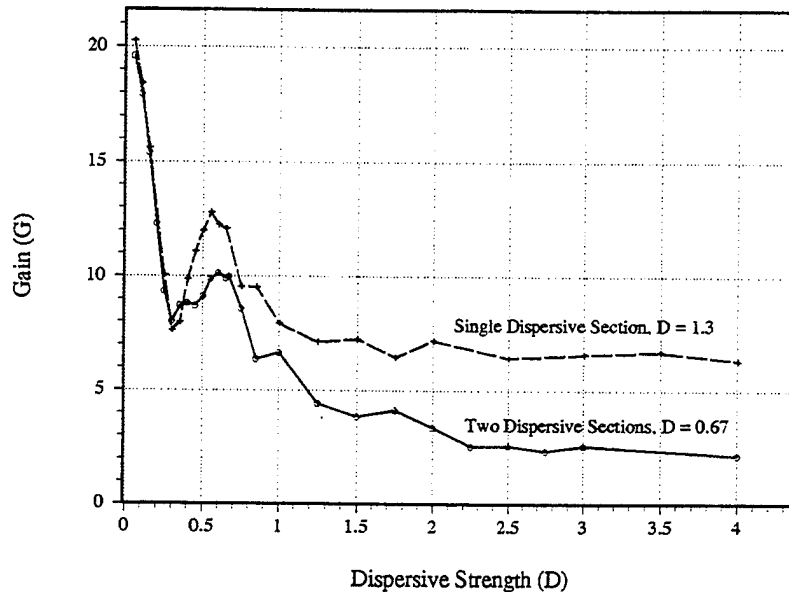
Figure 17. Single pass maximum gain vs. dispersive strength for a three-section klystron and a two-section klystron FEL with an initial dimensionless optical field strength of $a_0 = 10$.

So far, only the effects of dispersive sections on the maximum gain in a single pass have been shown. In Fig. 16, the cumulative effects of multiple passes may be extrapolated. As the optical field strength increases, each of the three example oscillators have a different rate at which the gain is reduced. If Fig. 16 is expanded so that the point at which each oscillator has a gain of unity can be determined, the results are not as one might expect at first glance. The three-section klystron is the first oscillator to reach a maximum gain of unity as the optical field is increased. The oscillator without the dispersive section is next to reach a gain of unity. The slope of the curve for each oscillator design is different as it crosses the $G = 1$ line and is not constant as the optical field increases. The region about which the oscillators reach $G = 1$ is between $a_0 = 44$ and $a_0 = 51$. This would lead to the conclusion that the

ln(1+G)

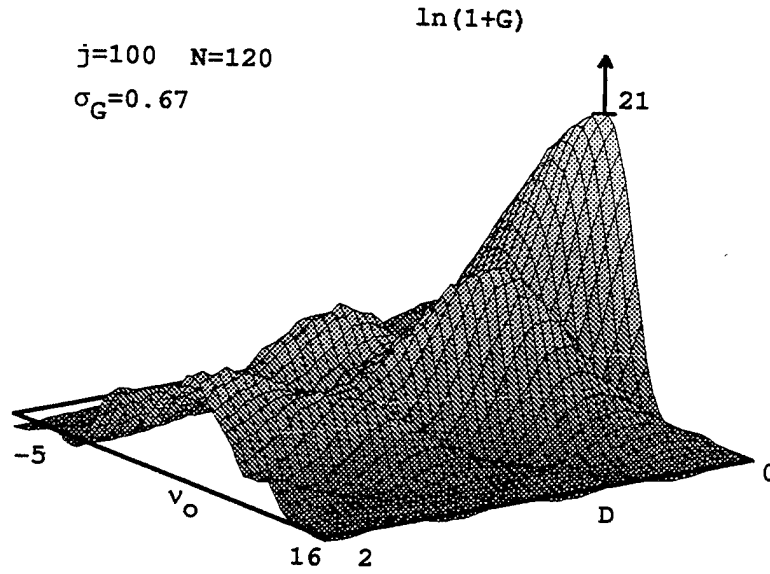j=100 N=120

σ_G=0.67

21

-5

ν_0

0

D

16 2

Figure 18.   Single pass gain spectrum as a function of dispersive strength, D, for a two-section klystron FEL.

steady-state optical field strength after many passes may be significantly different in each of the oscillators.

Figures 19, 20, and 21 show the evolution of the optical field after 2000 electron pulses have been passed through each oscillator. Two new FEL parameters are introduced at this point, desynchronism and slippage distance. Desynchronism and slippage distance may be understood by following the optical field through a full pass through the undulator from the point at which it encounters the first electron pulse to the next electron pulse. When the electrons have a phase velocity of $\nu_0 = 0$, they are said to be at resonance. This means that for every undulator period, they slip back along the light wave by one wavelength of light. This results in the electron beam falling behind the optical field by a distance of $N\lambda$ as it travels the entire length of the undulator. The normalized length of the electron pulse is $\sigma_z = l_e/N\lambda$, where l_e is the length of the electron pulse. Thus a slippage distance characterized by $\sigma_z < 1$ means

46

that the electron beam has slipped back along the optical field a distance that is greater than the length of the electron micropulse. This results in distortion in the shape of the optical pulse since the electron beam is not interacting with the same point in the optical field as it travels down the undulator. As the electron beam slips back along the optical field, the optical field grows stronger farther back along the length of the optical pulse. If a correction is not implemented, this will result in an optical pulse skewed towards the beginning of the undulator. This effect is corrected by introducing desynchronism. A desynchronism of $d = 1$ would mean that the electron pulse is injected into the undulator so that it is one slippage distance ahead of the optical pulse relative to the position it was introduced into the previous pass. Positive desynchronism is accomplished by increasing the length of the resonator cavity by a small fraction of the slippage distance so that the optical pulse arrives late with respect to the electron micropulse. Values of desynchronism are typically less than 1% of the slippage distance. Negative values of desynchronism are used in some applications [10].

Figures 19, 20 and 21 contain a large amount of information in ten different plots. The plot on the bottom left gives an indication of how far the electron beam slips back along the optical field in each pass relative to the length of the electron pulse where z is measured relative to the optical field in slippage distances. The dark curve is the electron pulse at the beginning of the undulator and the light gray shape is the electron pulse at the end of the undulator. The difference in the position of the electron pulse from the beginning to the end of the undulator is $\Delta z = 1$, the slippage distance, or approximately $1/\sigma_z \approx 25\%$ of the length of the electron pulse for SELENE. The plot in the center on the bottom is the weak field gain spectrum for the initial conditions of the oscillator. The plot on the bottom right is the power, P, in the optical field at the end of each pass. The power is the average of $|a(z)|^2$ over the entire window shown in the upper-left corner. When this plot is level over many passes, the oscillator may be considered to be in steady state.
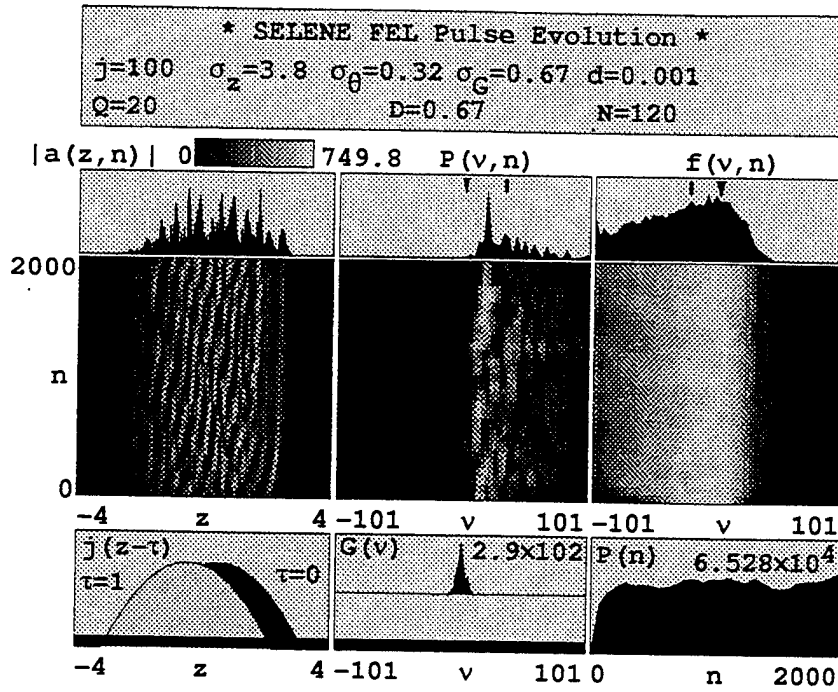
```
* SELENE FEL Pulse Evolution *
J=100    σ_z=3.8  σ_θ=0.32 σ_G=0.67 d=0.001
Q=20              D=0.67          N=120
```

|a(z,n)| 0 ▓▓▓▓ 749.8   P(v,n)   f(v,n)

2000

n

0

-4   z   4 -101   v   101 -101   v   101

J(z-τ)   G(v)   2.9x10²   P(n)   6.528x10⁴
τ=1   τ=0

-4   z   4 -101   v   101 0   n   2000

Figure 19.   FEL output parameters after 2000 electron pulses for a three-section
optical klystron oscillator.

The three middle plots show the development of the FEL over many passes. The left plot demonstrates how the optical field develops. The striated features indicate that the shape of the optical field is no longer smooth. The middle plot shows the power distribution as a function of the phase velocity of the electrons and the number of passes. The right graph shows the distribution of the electrons at the end of each pass as a function of phase velocity. From this, it can be seen that the oscillator with the single dispersive section is more efficient than the other two configurations at bunching the electrons.

The three plots at the top of Figs. 19, 20 and 21 show the optical field, power, and electron distribution at the end of the last pass. The two symbols at the top of the power and electron distribution graphs show the average distribution of these two functions. The triangle indicates the average for the first electron pulse. The line
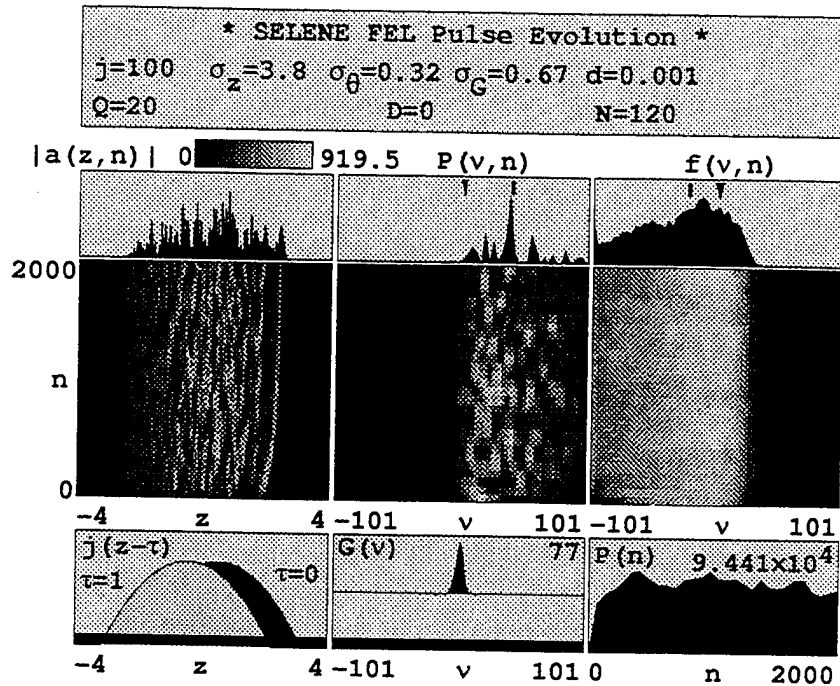
48

Figure 20. FEL output parameters after 2000 electron pulses for a single undulator oscillator.

indicates the average at the end of the last pass. The scale figure for the optical field strength, located in the upper-left corner, indicates that the maximum optical field strength is plotted in light gray, while the minimum optical field is plotted in black. This scale applies for the power and electron distribution graphs, but it is normalized for each application.

Figures 19, 20 and 21 indicate that if the damage threshold of the mirrors is sufficient, the SELENE parameters could provide a peak dimensionless optical field strength greater than 700. This results in a peak power density in excess of 24 MW/cm^2. The three-section klystron does have the lowest peak optical field strength, while the undulator without the dispersive section has the highest. The value of the optical field given by the scale is the maximum optical field strength developed during the entire run at any position along the optical wave. It is very easy to see that
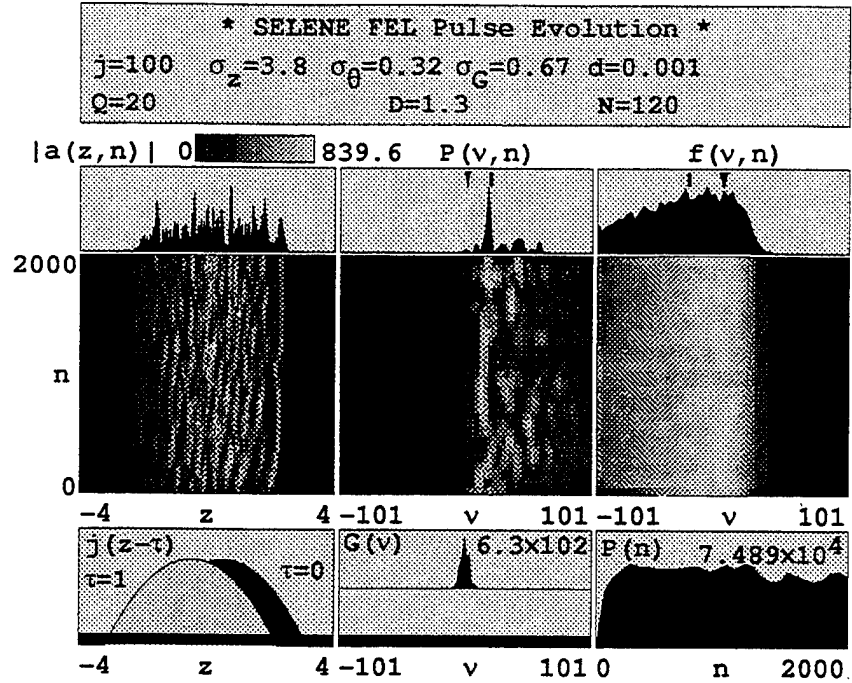
49

Figure 21. FEL output parameters after 2000 electron pulses for a two-section optical klystron oscillator.

the shape of the optical wave is definitely not a uniform or smooth waveform. This is due in particular to the high optical field strength and large electron current interacting in the undulator. The process of over bunching results in small pockets of electrons along the length of the optical wave which produce local amplifications much greater than the average, and thus the sharp peaks are found along the optical wave. The presence of the dispersive section in strong optical fields tends to aggravate this problem.

E. SELENE OPTIMIZATION

From Figs. 19, 20, and 21, it is easily seen that the current design of the SELENE project produces too much gain in the oscillator, as the optical field produced at steady state is much too high ($a \approx 750$) for current mirror technology as

well as producing an ill-conditioned electron beam for the radiator. Guided by the basic principles of FEL design, it is desired to retain the basic SELENE structure while finding ways to reduce the optical field in the oscillator. This must be accomplished while maintaining the function of the oscillator, which is to prepare the electron beam for the radiator. Several parameters may be varied in the design of the oscillator without incurring unusual deviations from the original design. Three of these parameters will be used to find a method which will reduce the peak optical field in the SELENE oscillator.

Desynchronism is one useful way of reducing the output power of the oscillator. The purpose behind desynchronism is to try and maintain the shape of the optical field as it propagates down the undulator. The top left-hand plot in Fig. 22 shows the effects of electron slippage on the shape of the optical pulse. As the electrons slip back along the optical pulse each pass, the trailing edge of the pulse is amplified more than the forward edge.

Introducing desynchronism also produces a reduction in gain. As the electrons are moved ahead of the optical field (positive desynchronism) or behind the optical field (negative desynchronism) some of the electrons are moved out of the interaction region early in the undulator and thus do not contribute to the initial gain in the undulator. When introducing desynchronism to the SELENE oscillator design, it is imperative that the function of the oscillator be maintained. As electrons are moved out of the optical field, the ability of the oscillator to bunch the electrons is reduced. Figure 23 shows the peak optical power density at the oscillator mirrors for various values of both negative and positive desynchronism. The optical power density is normalized to 9 MW/cm^2 on the vertical axis, which is equivalent to a peak dimensionless optical field of 424. In order to reduce the optical power density to 50 kW/cm^2, the amount of desynchronism would have to be in excess of 20% of a slippage distance (0.2 on the horizontal scale), or 24 optical wavelengths, in advance of the optical field. Typical values of desynchronism are on the order of less than 1%
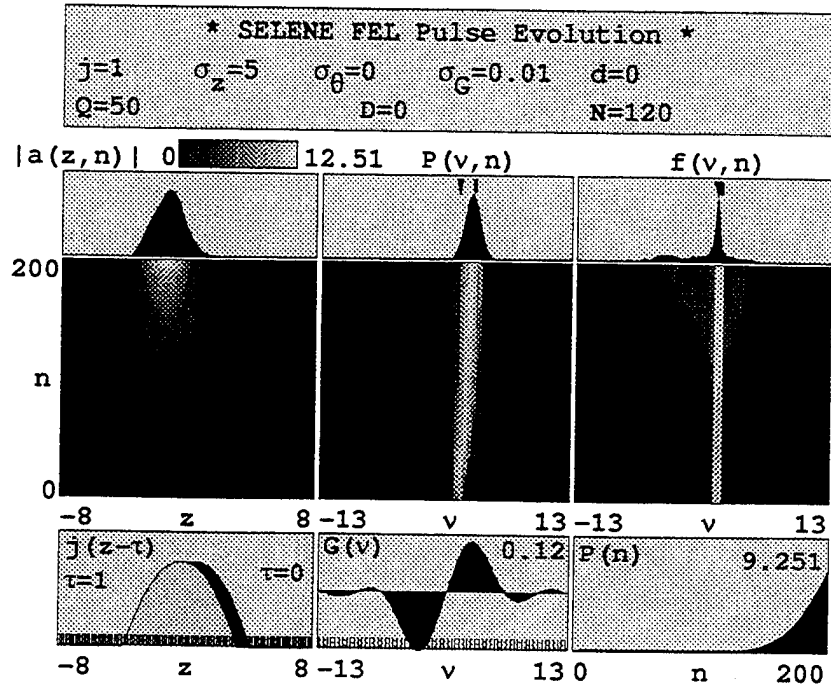
Figure 22.   Optical field evolution over 200 passes for a low current FEL. Parameters: $j = 1.0$; $\sigma_z = 5$; $\sigma_G = 0.01$; $d = 0$; $Q = 50$; $D = 0$.

of a slippage distance. Even out to 20% desynchronism, the optical power density is in excess of $1.2\ \mathrm{MW/cm^2}$, well above the limitations on the mirrors. Desynchronism, by itself, will not solve the problem of excessive gain in the SELENE oscillator. Using a desynchronism of 0.8% provides the lowest power output near the typical (1%) desynchronism level while still maintaining the function of the oscillator in bunching the electrons.

Another way to reduce the optical power in the oscillator is to change the losses in the oscillator. The major loss in an oscillator is the semi-transparent mirror which allows the laser light to leave the oscillator. Increasing the percentage of light removed from the oscillator each pass will result in a lower steady state optical field in the oscillator. For $Q = 20$, only 5% of the optical field power is transmitted through the
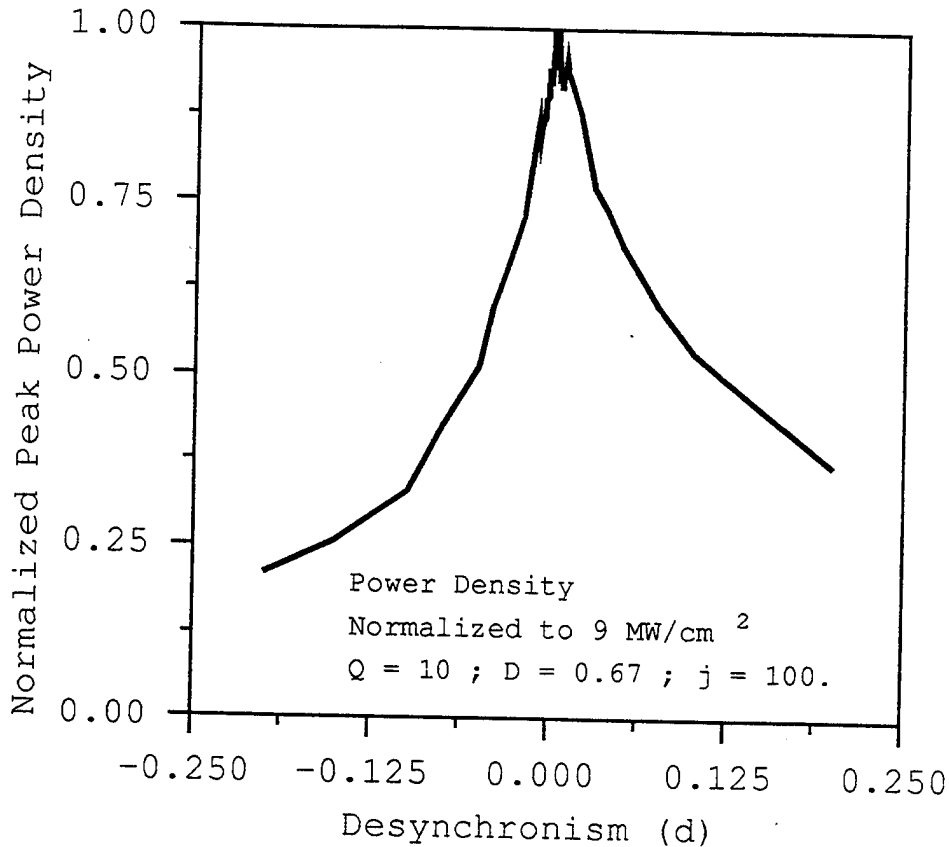
Figure 23. Normalized power density of the SELENE oscillator as a function of desynchronism, d.

semi-transparent mirror. This value of Q is a typical value to use for FEL's. Figure 24 shows the result of reducing Q in the SELENE oscillator. The plot is normalized to a peak power density of 19 MW/cm^2. The optical power is nearly linearly proportional to Q from $Q = 20$ down to a value of $Q = 2.5$. Figure 25 is an expansion of Fig. 24 which shows the relationship between optical power density and Q for $Q < 1$. In order to reduce the optical power density below 50 kW/cm^2, Q must be reduced below 0.25. This means that a transmittance $(1 - e^{-1/Q})$ of 98% is required in the output mirror. As can be seen from Fig. 25, the optical power drops rapidly for $Q < 0.25$. This is to be expected as the gain in the oscillator is no longer able to makeup for the losses in the cavity and the oscillator essentially becomes a radiator. $Q = 5$ is chosen

for a reasonable compromise between maintaining low optical power and keeping optical characteristics of the mirrors in a reasonable range. This results in a 20% transmittance for the output mirror.
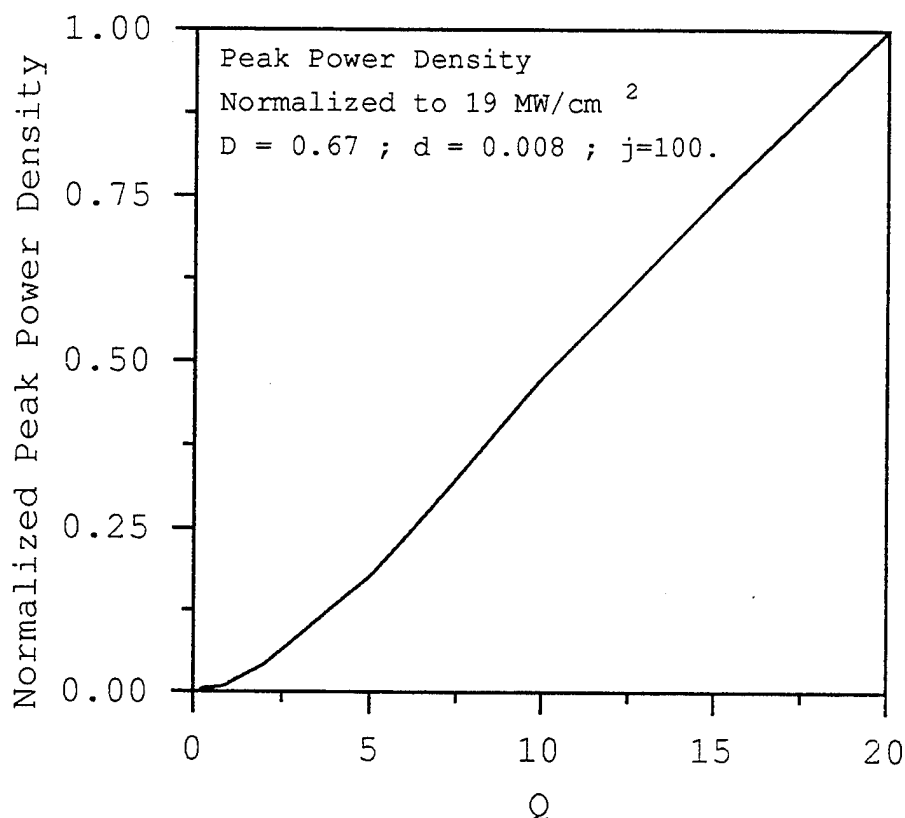

Figure 24. Normalized power density of the SELENE oscillator as a function of Q.

The original design of SELENE exploited the effect of optical klystrons in strong optical fields. The dual dispersive section results in the ability to change the relative strength of the dispersive sections and to allow for some inherent flexibility in the design of SELENE. As previously shown in Fig. 17, the single pass gain for an optical klystron is not much affected by changes in dispersive strength for $1 < D < 4$. This can be understood by looking at the effect of the dispersive section on the electron beam in strong optical fields. In strong optical fields, the electrons are bunched prior to entering the dispersive section. If the electrons are already bunched prior to
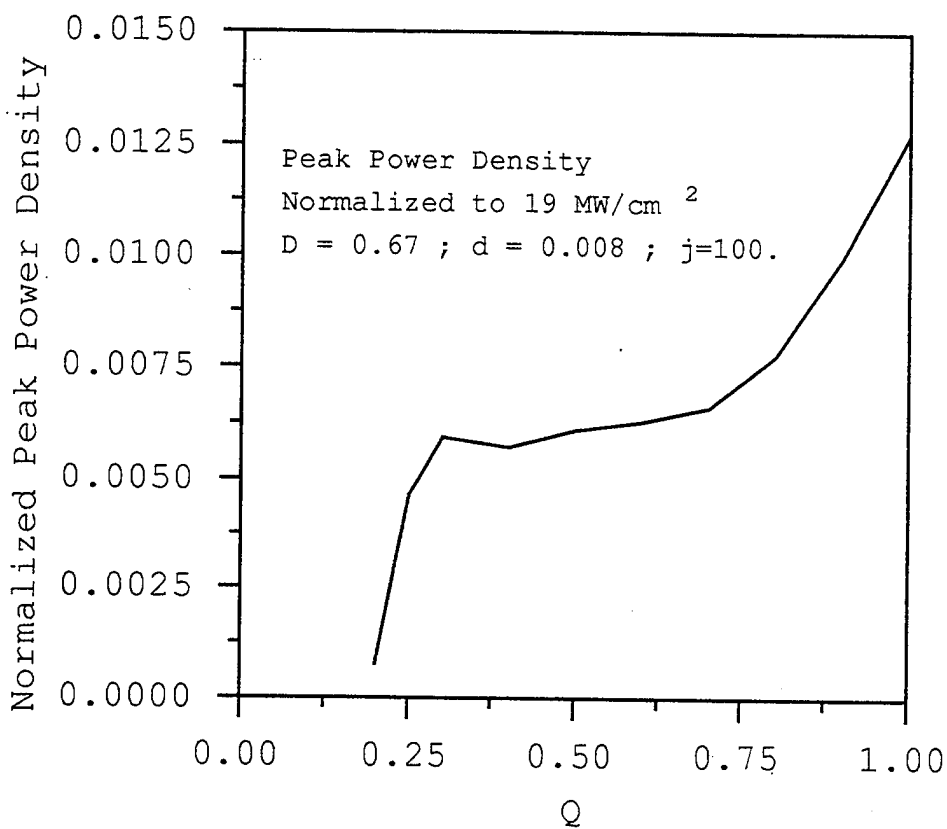
Figure 25.   Normalized power density of the SELENE oscillator as a function of Q for $Q < 1$.

entering the second undulator section, they will be severely dispersed in the dispersive section. For small values of D, this dispersive effect is proportional to the dispersive strength. For larger values of D, the dispersion results in a nearly random distribution in the electrons' phase; thus increasing the dispersive strength will result in little reduction in the single pass gain.

For SELENE, the steady state optical field strength is strong enough to over-bunch the electrons prior to reaching the first dispersive section. As can be seen in Fig. 26, increasing the dispersive strength of the dual klystrons will not result in a significant reduction in the optical power at the mirrors. Thus, with reasonable

55

selections of parameters, the excessive gain in the SELENE oscillator cannot be defeated. The main function of the oscillator is also defeated in the current design. Figure 27 shows the electron distribution in phase-space when they exit the oscillator. Instead of bunching the electrons for the radiator, the oscillator has essentially produced an electron beam of the same current, but with a much larger energy spread. This is a direct result of the strong fields combined with an optical klystron in the oscillator.

<figure>
Y-axis: Normalized Peak Power Density (1.00, 0.75, 0.50, 0.25, 0.00)
X-axis: Dispersive Strength (D) (0.0, 0.5, 1.0, 1.5, 2.0)

Peak Power Density
Normalized to 2.8 MW/cm ^{2}
Q = 5 ; d = 0.008 ; j = 100.
</figure>
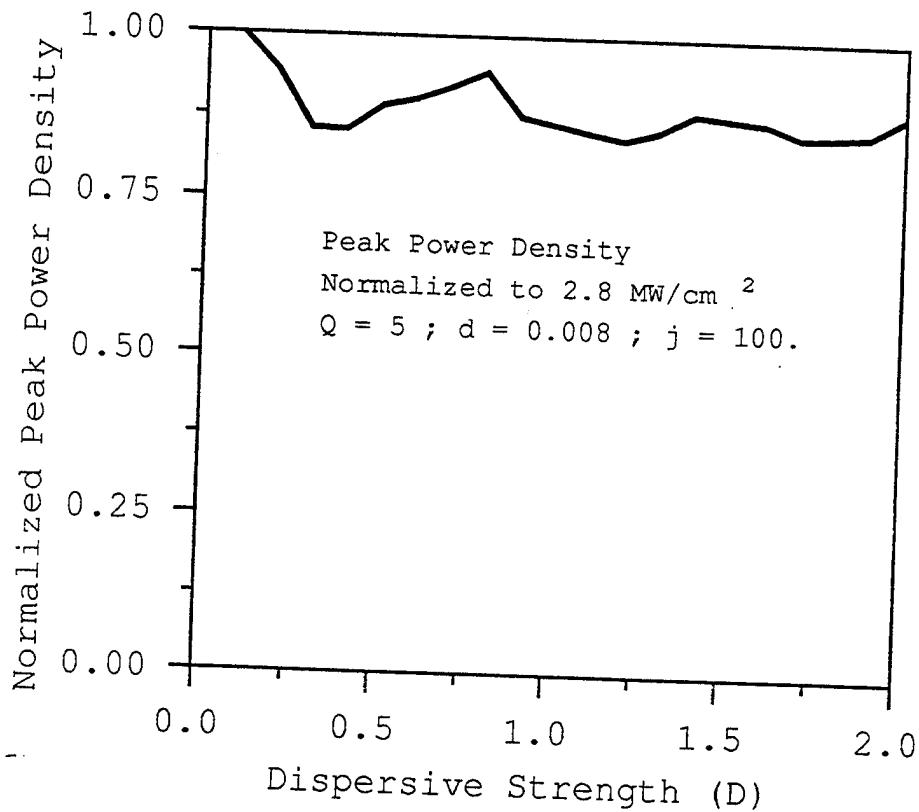
Figure 26.   Normalized power density of the SELENE oscillator as a function of the dispersive strength, D.

In order for the oscillator to bunch the electrons properly, the optical field must be reduced, and the dispersive sections must be tailored to the specific purpose of the oscillator. Using the dispersive section to reduce the optical field may actually hinder
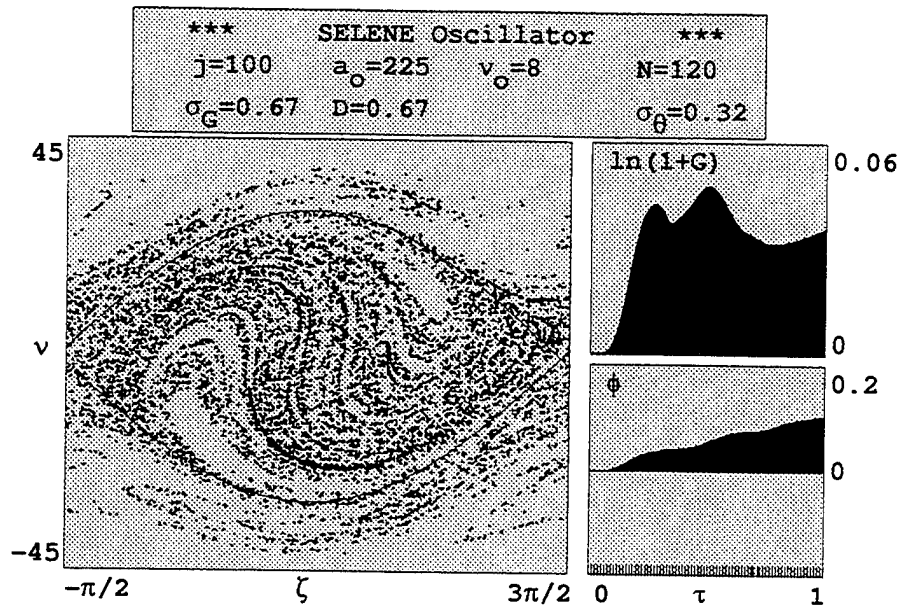
Figure 27. Phase-Space plot of the electron distribution exiting the SELENE oscillator.

the ability of the oscillator to bunch the electrons for the radiator. The current oscillator design does not adequately bunch the electrons, which leads to an exploration of possible alternative designs for the SELENE oscillator.

IV. ALTERNATE PROPOSALS FOR THE SELENE OSCILLATOR

A. INTRODUCTION

In the previous discussion of the oscillator design for SELENE, some of the different effects of a single dispersive section and single undulator design were demonstrated. Figure 16 shows that there is a significant loss of gain when only one dispersive section (instead of two) is used in weak optical fields. Figure 17 demonstrates that this may no longer be the case for strong field FEL's. In order to keep the flexibility of design inherent in the use of an optical klystron, the two-section optical klystron will be investigated as a first attempt to allow the SELENE oscillator to perform properly.

B. TWO-SECTION OPTICAL KLYSTRON ALTERNATIVE OSCILLATOR DESIGN

Figure 21 shows that just using a single dispersive section in the same undulator design will still produce excessive gain and strong optical fields ($a \approx 840$). Thus, the need to reduce gain leads to the necessity for a shorter undulator. Reviewing the previous discussions of the relevant parameters leads to the proportionalities,

$$\sigma_G \propto N \ ,$$
$$\sigma_\theta \propto N \ ,$$
$$\sigma_z \propto \frac{1}{N} \ , \tag{4.1}$$
$$j \propto N^3 \ ,$$
$$|a|_{max} \propto \frac{1}{z_0} NL |\vec{S}|_{max}^{1/2} \ .$$

In order to determine the length of undulator desired for the two-section oscillator, the best parameter to use is the dimensionless current density. With low current

59

conditions, the gain in a single pass undulator is given by $G = jD/4$. Thus with $j = 1$, the gain in a single pass is $D/4$. With proper choices for desynchronism and resonator losses small values of D may enable the oscillator to remain in the weak field regime. Using Eq. 4.1, the parameters used to describe the electron beam distribution and slippage distance for $j = 1$ are $N = 26$, $\sigma_G = 0.15$, $\sigma_\theta = 0.07$, and $\sigma_z = 17.5$. Again assuming the mirrors are designed to produce a Rayleigh length equal to the length of one undulator section, $z_0 \approx 1.1$ m. This will result in a maximum dimensionless optical field strength of $|a|_{max} = 4.6$ in order not to exceed 50 kW/cm^2 at the mirrors, keeping the mirror separation distance at $S_m = 79$ m.

Figure 28 is a plot of the normalized peak power density after 1000 electron pulses as a function of desynchronism. The peak power density is normalized to 211kW/cm^2. As before, negative desynchronism results in the greatest decrease in optical power for small changes in desynchronism (steepest slope). However, negative desynchronism will prevent a larger number of electrons from interacting with the optical field. For $d > 0$, the peak power density decreases as desynchronism is increased. Thus a small value of positive desynchronism of $d = 0.02$ is best, in this case, to ensure the largest number of electrons continue to interact with the optical field while allowing for a small reduction in the steady state optical field strength.

After determining the desynchronism to be used in this two-section oscillator, the next step is to determine the dispersive strength which will optimize the performance of the oscillator and reduce the optical field. Figure 29 is a dual plot showing the normalized peak power density and the normalized peak dimensionless optical field strength as a function of dispersive strength, D. The peak power density is normalized to 284 kW/cm^2 and the peak dimensionless optical field strength is normalized to $|a| = 11$. The peak power is seen to be reduced as the dispersive strength is increased. The peak dimensionless optical field strength follows a similar reduction until $D > 0.3$. At this dispersive strength, the optical field tends to be
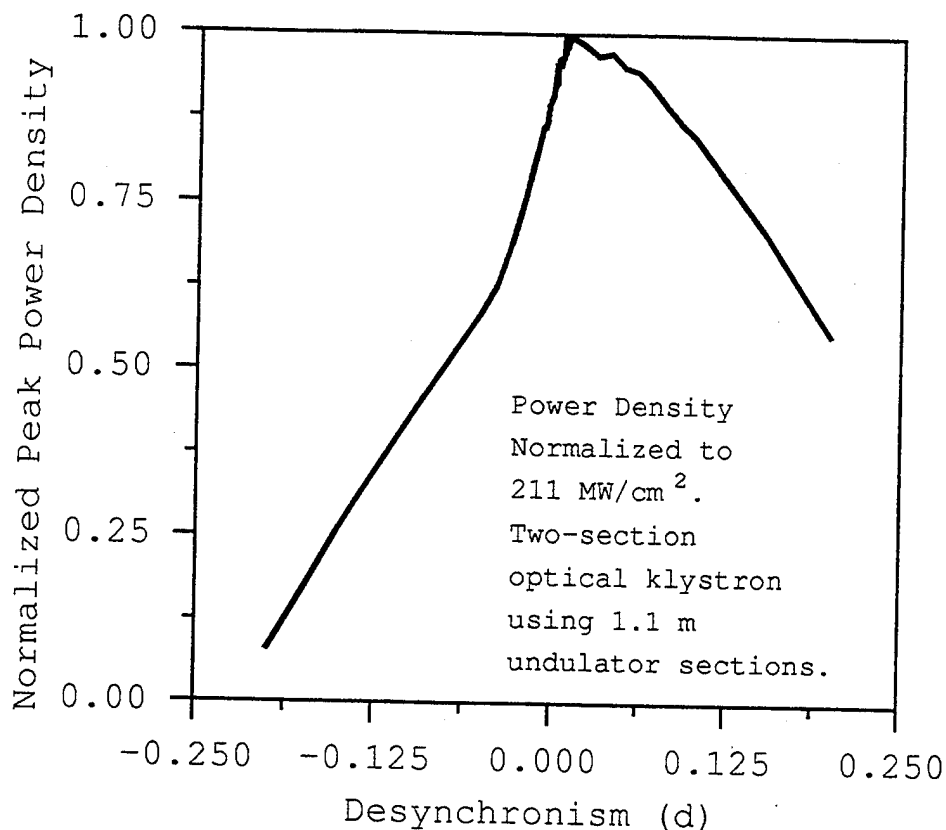
Figure 28. Normalized peak power density as a function of desynchronism for the two-section optical klystron configured for $j = 1$.

reduced much more slowly than the peak optical power. This can be explained using Figs. 30 and 31.

Figure 30 shows the optical pulse evolution over 3000 passes. It can clearly be seen from the upper left-hand plot, that the optical pulse shape is smooth and nearly symmetrical. An increase in the peak optical field strength with this optical envelope shape will be accompanied by an increase in the average power in the oscillator. However, Fig. 31 shows the same oscillator with a dispersive strength of $D = 0.4$. In this figure, the reason for the discrepancy in Fig. 29 becomes apparent. The stronger dispersive strength in the presence of strong optical fields tends to produce many small areas of bunching along the optical pulse and therefore, the optical field is
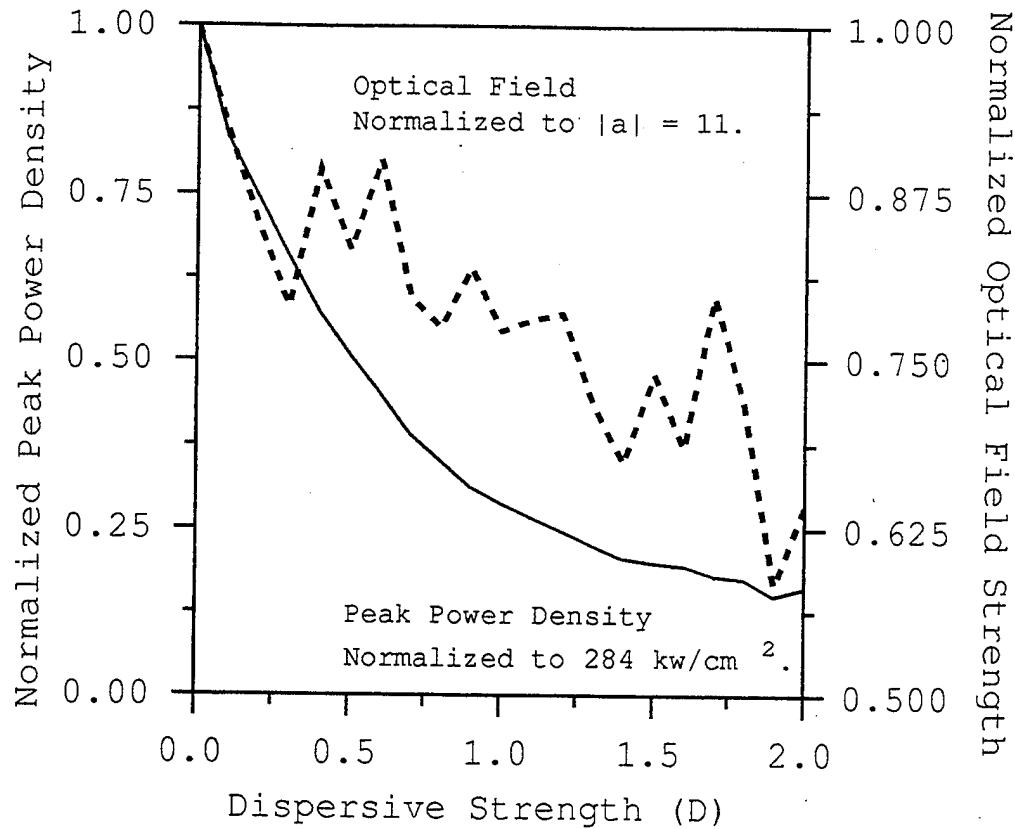
Figure 29. Normalized peak power density and optical field strength as a function of dispersive strength for the two-section optical klystron with $j = 1$.

amplified in a non-uniform manner. This causes the spikes in the optical field envelope. This can be avoided by using lower values of dispersive strength, or lowering the optical field. For this situation, the aberrations in the optical field envelope lead to the decision to choose $D = 0.3$ for a dispersive strength. This will produce a decrease in power density to $\approx$ 65% of the steady state power density attained without the dispersive section, or to 185 kW/cm^2. Thus, a decrease in the dimensionless optical field strength by a factor of two is still necessary in order to prevent damage to the mirrors in the oscillator.

Figure 32 shows the normalized peak power density as a function of Q. The power density is normalized to 177 kW/cm^2. The optical field intensity is reduced
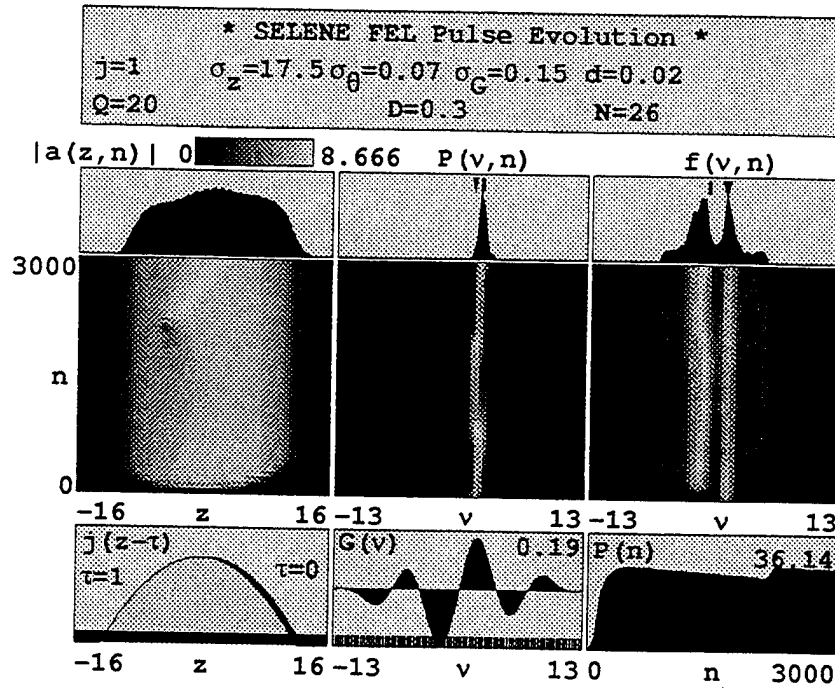
Figure 30. Optical pulse evolution during initial 3000 electron pulses. $D = 0.3$ for the two-section optical klystron.

rapidly as the resonator losses are increased. For $Q < 6.6$, the undulator gain is insufficient to make up for the resonator losses. If the FEL oscillator output mirror is chosen such that $Q \approx 7$, then the dimensionless optical field strength is low enough to prevent damage to the mirrors in the oscillator. This seems to be a reasonable proposal to allow the oscillator to work but not damage the mirrors in the oscillator. However, the function of the oscillator must be considered.

Figure 33 shows the phase-space plot for the electrons at the end of the oscillator. The electrons plotted in light gray are the positions of the electrons just prior to the dispersive section. The electrons plotted in dark gray are the positions of the electrons as they exit the undulator. As can be seen in comparison with Fig. 11, the dispersive section acts to bunch the electrons. Since the initial optical field is not strong enough to have over-bunched the electrons prior to the dispersive section, the
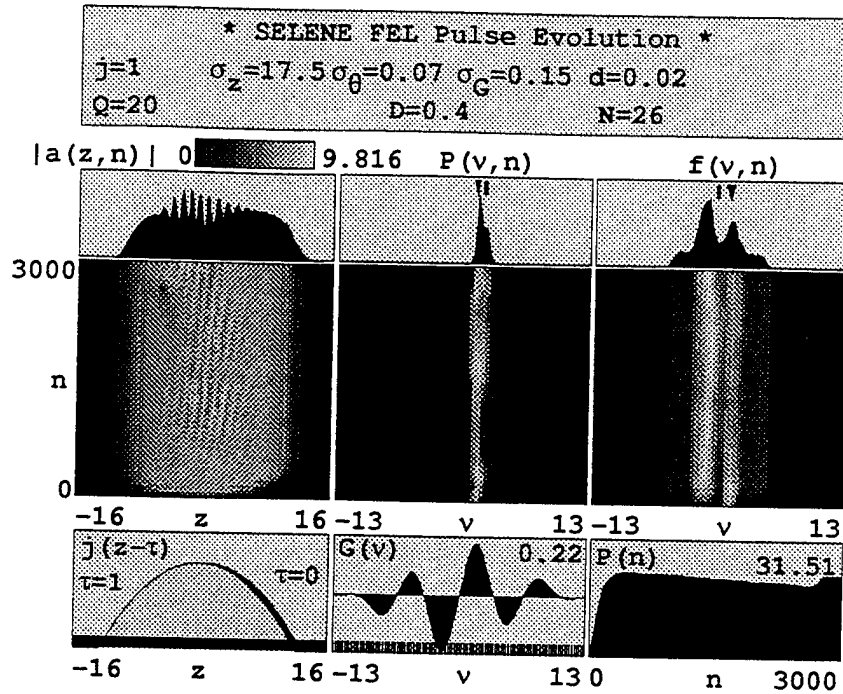
Figure 31. Optical pulse evolution during the initial 3000 electron pulses with $D = 0.4$ for the two-section optical klystron.

dispersive section in the oscillator bunches the electrons and the second undulator section continues to interact with the optical field and the results are seen in Fig 33.

At first glance, the objective of the oscillator seems to have been met. The electrons are bunched at the end of the oscillator and the mirror damage threshold is not approached. However, there is still the small dispersive section between the oscillator and the radiator to consider. As previously discussed and shown in Fig 13, having the electrons bunched prior to entering a dispersive section results in the electrons being dispersed instead of bunched. This will result in reduced efficiency in the radiator in extracting energy from the electron beam. If, however, upon exiting the oscillator, the electron beam could look similar to the electrons plotted in light gray in Fig 33, then the dispersive section between the oscillator and the radiator will bunch the electrons and the radiator efficiency will be increased dramatically. This may be
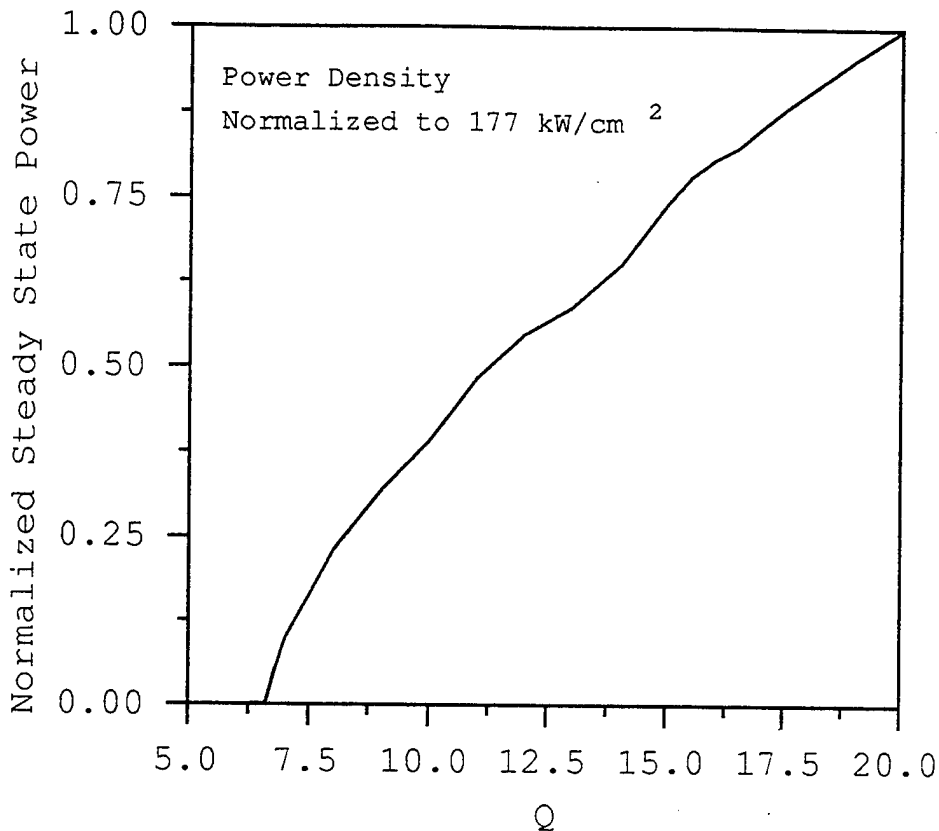
Figure 32.   Normalized steady state power density as a function of Q for the two-section optical klystron configured for $j = 1$.

accomplished by removing the dispersive section in the oscillator and reducing the dimensionless optical field strength to the weak field regime.

C.   SINGLE UNDULATOR ALTERNATIVE OSCILLATOR DESIGN

As stated before, removing the dispersive section from the previous oscillator design is not sufficient to provide the electron beam conditioning desired for the radiator. The presense of strong optical fields will result in the electrons being bunched prior to leaving the oscillator. The condition desired is similar to Fig. 4. The sinusoidal shape of the phase-space plot is the most desirable condition for the electron beam to exit the oscillator. This particular proposed design will result in the
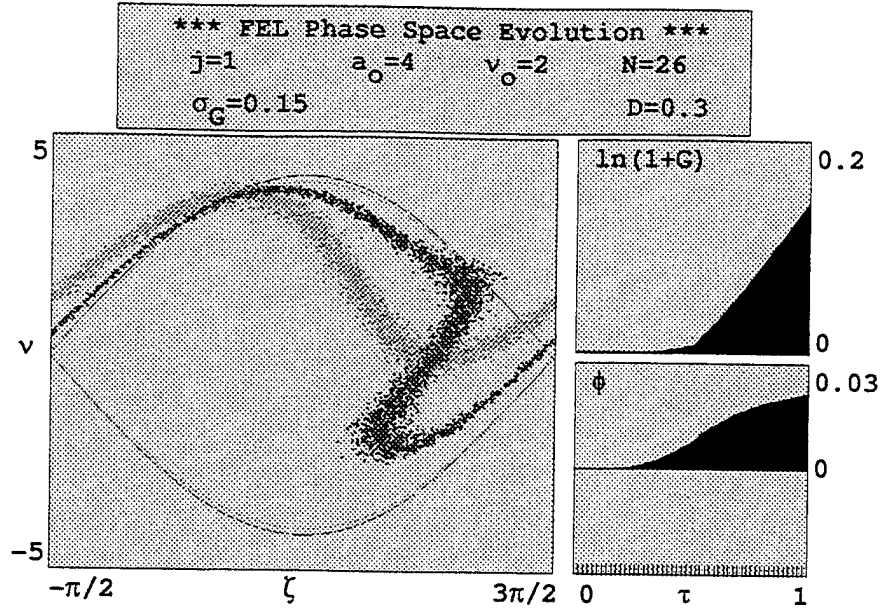
Figure 33. Phase-Space plot for the two-section optical klystron.

electron beam being bunched prior to entering the radiator instead of at the exit of the oscillator. In order to reduce the optical field to the weak field regime, the previous design, without the dispersive section and a lower Q could be used. However, using a lower value of Q will tend to make the oscillator unstable. As can be seen in Fig. 32, the output power is sensitive to changes in resonator losses near the value which will produce the required weak optical field. In order to save the cost of constructing a larger undulator for the oscillator, and to try and find a less sensitive solution, the undulator may be shortened.

An undulator length of 2 m is a reasonable solution to this problem. With this design, and using Eq. 4.1, the electron beam parameters are $N = 22$, $j = 0.6$, $\sigma_G = 0.12$, $\sigma_\theta = 0.06$, $\sigma_z = 21$, and $|a|_{max} = 2.0$. Again, desynchronism and resonator losses will play an important part in this design. Figures 34 and 35 are indications of why these two factors are so important. In Fig. 34, the combination of resonator losses and slippage results in the FEL failing to sustain itself. The gain is small

66

compared to the original design of the SELENE oscillator. The interaction distance is also short, thus making the slippage of the electron beam along the optical beam an important feature. In the beginning of a simulation of this type, the optical field is seeded with a weak field of strength $a_0 = 0.001$. Early in the evolution, the electron micropulse interacts with the optical field resulting in amplification of the field. Due to the slippage of the electron pulse, the optical field tends to be amplified along the trailing edge. Due to resonator losses, the overall gain for the oscillator is small. As seen in the middle-left plot, this makes the optical field "walk" backwards. After ≈ 1000 electron pulses, the optical field and the electron beam are no longer interacting sufficiently to produce gain in the optical field.
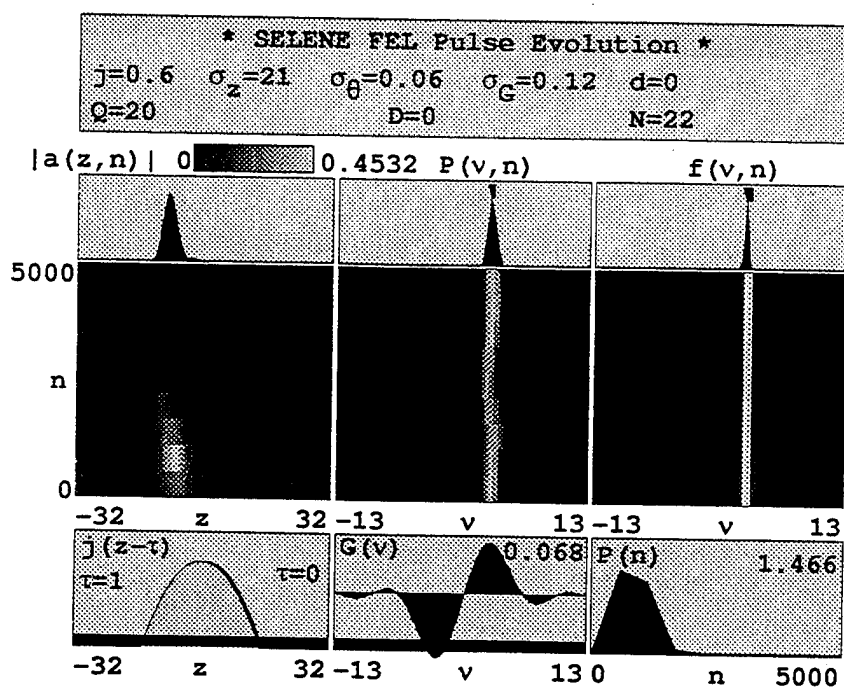

Figure 34.   Optical pulse evolution over 5000 electron pulses for the single undulator segment design with $Q = 20$ and $d = 0$.

In Fig. 35, the resonator losses are reduced so that $Q = 25$. This is sufficient to enable the electron beam to interact and produce a stable optical field over many

passes. However, the shape of the optical field is not optimum. This "shark-fin" shape will produce non-uniform bunching in the electron beam. Thus, the need for desynchronism. Due to the nature of the shape of the optical field, as desynchronism is increased, the magnitude of the peak optical field will have a small initial increase since a larger fraction of the electrons will spend time interacting with the peak optical field. As this happens, the optical wave shape will expand. Because of these two phenomena, as desynchronism is increased near $d = 0$, the peak optical field will remain relatively constant while the total power in the optical field increases significantly.
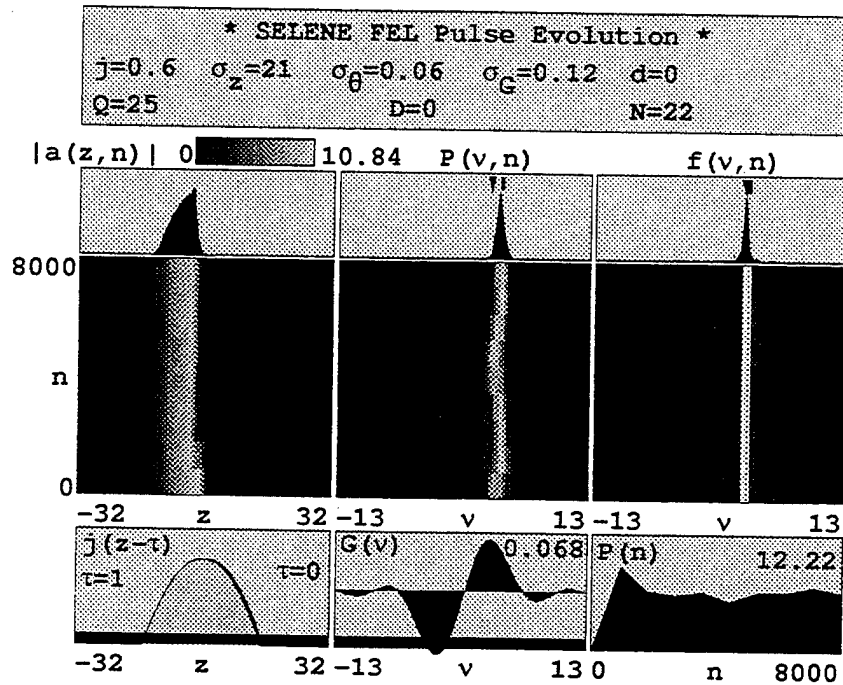

Figure 35.   Optical pulse evolution over 8000 electron pulses for the single undulator segment design with $Q = 25$ and $d = 0$.

This phenomenon will continue until a symmetric waveform is approached as in Fig. 36. At $d = 0.02$, the shape of the optical pulse is symmetric and uniform. Increasing desynchronism beyond this point will provide the same results as discussed

in previous sections. As desynchronism is increased, the peak optical field will decrease and the total power in the optical field will also decrease. Note that negative desynchronism in this case would be counter-productive as it would remove the electron pulse from the optical field envelope much sooner than without desynchronism. This will not produce a stable optical field and is not a choice for this system. Starting with the uniform optical field envelope from Fig. 36, Fig. 37 can be constructed. Figure 37 is a plot of peak optical field strength as a function of Q. With $d = 0.02$, the shape of the optical field pulse remains consistent as Q is decreased. At $Q = 13.8$ the peak optical field strength is reduced below $|a| = 2$ which will prevent damage to the conservative mirror elements. This also is in the weak field regime.
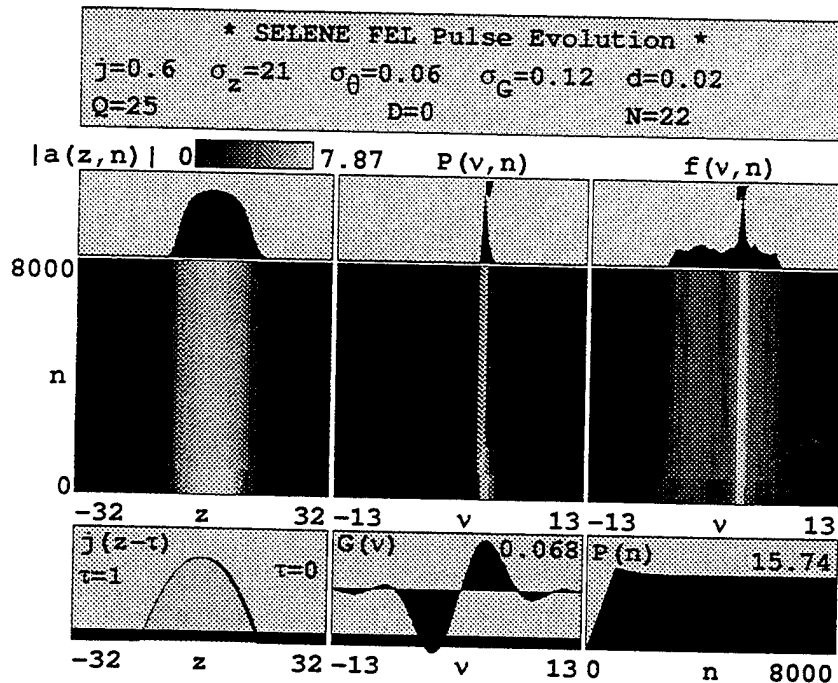

Figure 36. Optical pulse evolution over 8000 electron pulses for the single undulator segment design with $Q = 25$ and $d = 0.02$.

Figure 38 is the phase-space plot of the electrons exiting the oscillator cavity with an optical field strength of $a = 2.0$. This is the type of sinusoidal shape desired in
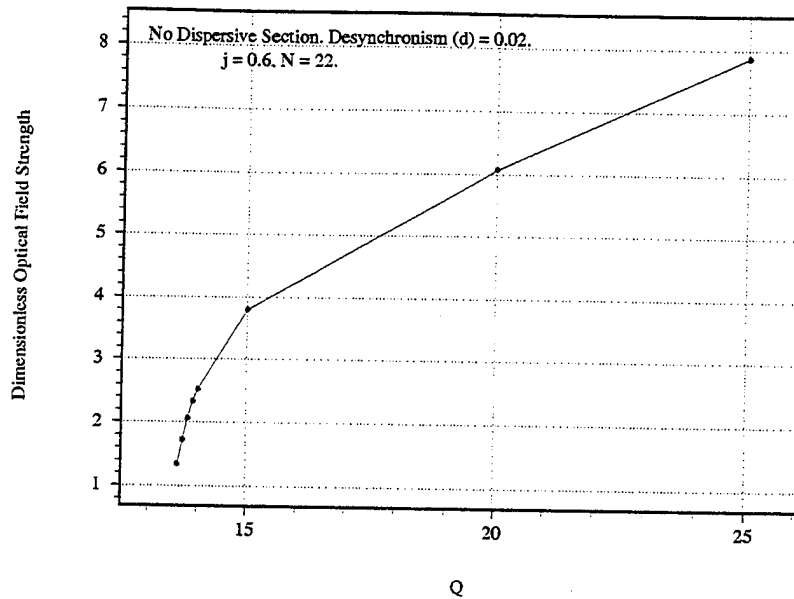
69

Figure 37. Dimensionless optical field strength as a function of Q for the single undulator segment design.

order to take advantage of the dispersive section between the oscillator and the radiator. However, it will be important to choose the dispersive section strength properly in order to continue the bunching process without overbunching. With the use of an achromatic bending system, the electron beam can be introduced into the radiator without any further bunching. A compromise between the achromatic bending and the current designed dispersive strength is required for optimum performance of the radiator.

For further consideration, the flexibility of this system can be expanded upon. With increasing advances in the design of optical devices, mirrors which can withstand greater than $200 kW/cm^2$ of incident optical power density may be available by the time the SELENE project is finalized. This will expand the region of acceptable resonator loss to $13.6 \leq Q \leq 15$. With the use of a feedback and control system, the desynchronism of the oscillator may be dynamically controlled. With the main purpose
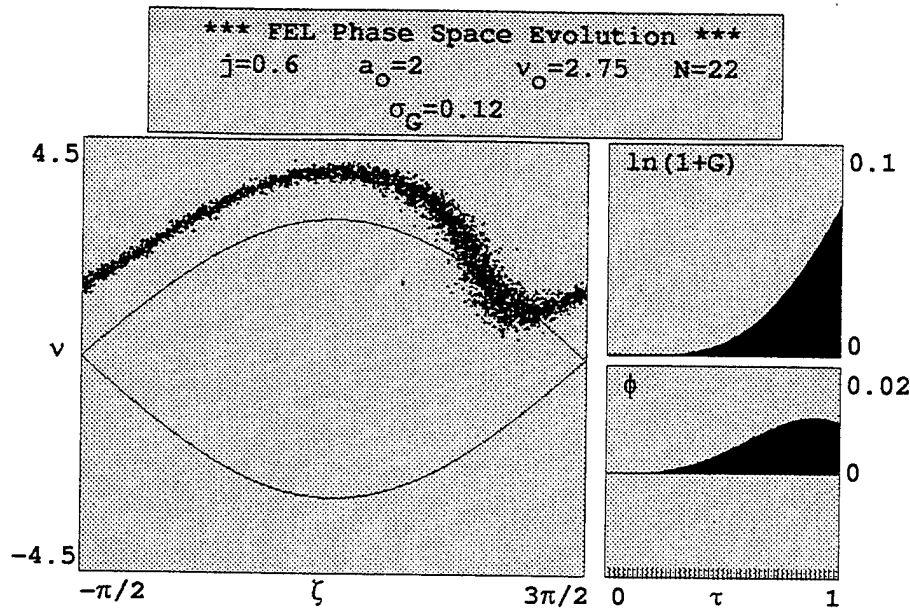
70

Figure 38.   Phase-Space plot for the electrons exiting the single undulator segment oscillator.

of the oscillator being to maintain weak field electron beam bunching, a feedback loop may be implemented to dynamically control the desynchronism to maintain the optical field in the weak field regime.

This feedback system can also be used in conjunction with a variable dispersive section system between the oscillator and the radiator. This design originally proposed for the dispersive sections inside the oscillator can be used to assist in dynamically controlling electron bunching. As the optical field strength decreases, the strength of the dispersive section can be increased to bunch the electrons prior to entering the radiator. As the optical field increases, the dispersive section can be made achromatic, in other words, non-dispersive. As the dimensionless optical field strength reaches $a = 4$, the dispersive section should be fully achromatic. With full use of an integrated feedback system, the output from the radiator can be optimized dynamically and thus the available power to the satellites will be maximized.

71

V. CONCLUSIONS

With the current explosion in electronics technology, the United States military services are developing a large arsenal of data gathering sensors and equipment. This data, in most cases is gathered in the field and needs to be transmitted to a coordinating unit for processing. Advances in optical devices and sensors are increasing the range and reliability of optical sensors in various ranges of frequencies from microwave to visual imaging. The number of sensors in the field which use video technology for relaying information is increasing rapidly. The communications requirement for the military services is expanding. The days of the walkie-talkie communications are numbered. All of these communications needs must be met. The bandwidth required to transmit video images on a real-time basis is an order of magnitude larger than that required to transmit voice. Navigation and precise positioning information is also necessary for current targeting data to prevent collateral damage. With the rapid proliferation of cellular phone systems, the commercial communications world is also expanding it's needs to provide world-wide continuous coverage for customers. All of these concerns have at least one thing in common. They all benefit from the use of satellites.

In the near future, a global telecommunications system will be installed using a series of satellites. The number of people requiring continuous Global Positioning System (GPS) service will rapidly expand as different applications are introduced into society. Currently, even some novice of fishermen have a GPS system on board mounted next to the fish-finder. In the near future, it can be imagined that cars can be programmed with a travel route and with the use of GPS and other appropriate sensors, a long arduous road trip may be made without error, and possibly without manual intervention. The newest television systems are using satellite technology to provide interactive programming directly to a small communications satellite dish. Because of the increasing reliance on satellite systems, and the increasing functional

requirement of these satellites, any method which will lower the orbital placement cost of new satellites, or extend the lifetimes of current satellites will be welcome by both industrial interests and by consumers. The military services, which use both special military satellites and commercial units, will benefit greatly from such an improvement. This advanced technology is the purpose of SELENE.

The United States and Russian governments have agreed to conduct a joint development of a ground-based, high-average-power laser system to provide electrical power to satellites in orbit. The design will use a Free Electron Laser (FEL) system. This FEL system consists of two main components in addition to the electron beam source: an oscillator, and a radiator. The electron beam will be provided by a 51 MeV race-track microtron recuperator. The electron beam will be injected into the oscillator which will bunch the electrons. The electrons will then enter the radiator where they will produce a coherent optical field by spontaneous emission. After the field is developed, it is further amplified by the interaction in the undulator between the electrons and the optical field. The resulting laser light is then transmitted through a two-mile-long vacuum chamber to allow it to expand before reaching the beam director. The beam director will reflect the laser beam to the satellites using adaptive optics techniques to compensate for atmospheric disturbances.

In order to provide high power from the radiator, the electron beam current must be large. In the oscillator, this causes several problems. Mirror damage is a concern since strong optical fields could be developed in the oscillator. These strong optical fields tend to destroy the bunching of the electrons as they travel down the oscillator. The original three-section optical klystron was used to try and reduce the strong optical fields in the oscillator. Chapter III discusses the proposed system for the SELENE oscillator and the limitations of the system. With current mirror technology, it is difficult to develop a stable, optical field using that system that will not exceed the damage threshold of the mirrors. Even if the mirrors could be designed to withstand the intense optical field produced by this oscillator, the purpose of the oscillator would not

74

be served for the following reason. Figure 13 shows the result of using dispersive sections in strong optical fields. The electrons are bunched prior to reaching the dispersive section. When the electrons exit the dispersive section, the electrons have been scattered instead of being bunched. SELENE has not just one, but two, dispersive sections operating in strong fields. The result is shown in Fig. 27. The electrons leaving the oscillator are not bunched. Instead, this combination of dispersion and strong optical fields produces a relatively uniform electron distribution in ζ with a much larger energy spread than the original electron beam. This will inhibit the creation of coherent radiation in the radiator.

As an alternative to the SELENE proposal, a two-section optical klystron was studied. The two undulator sections were shortened in order to reduce the dimensionless current density to $j = 1$. The resulting investigation showed that by proper selection of dispersive strengths, desynchronism, and resonator losses, the goal of weak field bunching in the oscillator could be met. However, this solution is very sensitive to resonator losses. The other concern is that even under the weak field conditions, the electrons are bunched when they exit the oscillator. The dispersive section between the oscillator and the radiator will again disperse the electrons instead of bunching them.

Another alternative to the SELENE proposal is to remove the dispersive section and shorten the undulator. At first, this configuration seems to require a large Q in order to produce a stable optical field. Once a value for resonator losses was found which allowed the production of an optical field, the shape of the optical pulse became an issue. Selecting a desynchronism value which optimized the shape of the optical field resulted in $d = 0.02$. With this desynchronism, the resonator losses were increased until a stable, weak optical field was formed. As Q was reduced, the number of passes required to form the optical field grew, but the optical field remained stable as the steady state dimensionless optical field strength was reduced to $a = 1.3$, well within the weak field range. For $13.5 \leq Q \leq 14.3$, the single section oscillator is

able to produce a stable weak optical field. In Fig. 39, the optical pulse evolution over 50,000 electron pulses is shown for $Q = 14$. The optical field stability in the weak field range allows for dynamic control of desynchronism and the strength of the dispersive section between the oscillator and the radiator.
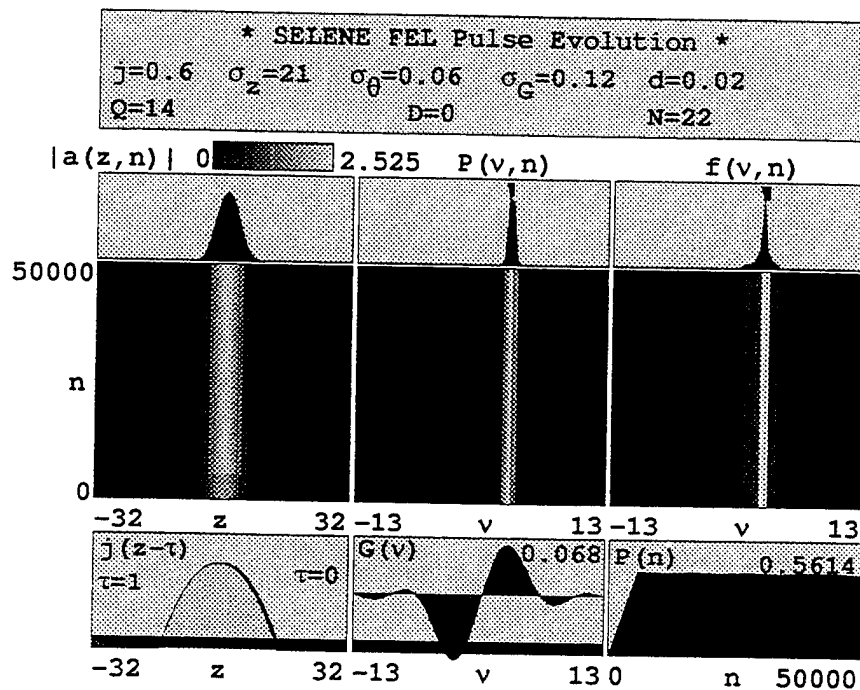

Figure 39.   Optical pulse evolution during 50000 electron pulses for the one-piece undulator.

Figure 40 demonstrates the usefulness of the dispersive section between the oscillator and the radiator. The left-hand side is the phase-space plot of the electrons as they exit the oscillator. The right-hand side is the phase-space plot of the electrons as they enter the radiator after passing through a dispersive section with $D = 0.25$. Note that the effect of the dispersive section in weak optical fields is to bunch the electrons. Because the radiator does not have an initial optical field, the relative phase at which the electrons are bunched is not important, just that they are bunched in phase as they begin to produce coherent radiation by spontaneous emissions.

*** FEL Phase Space Evolution ***
j=0.6   a$_o$=2.5   v$_o$=2.7   N=22
σ$_G$=0.12   D=0.25

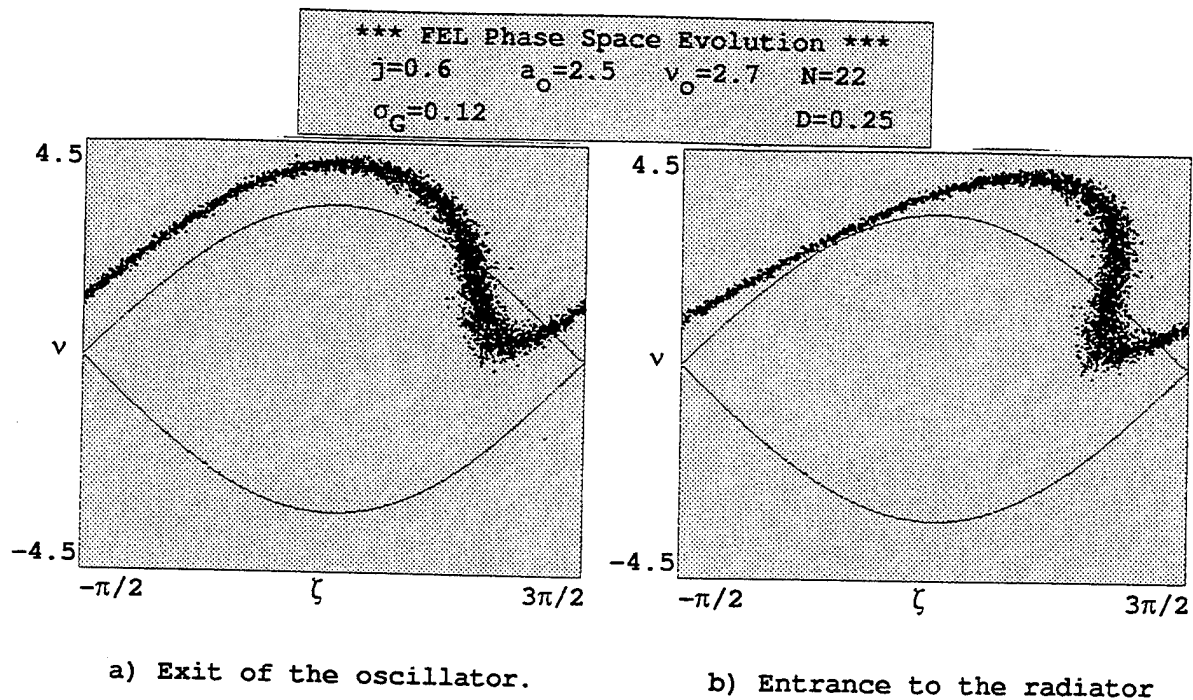a) Exit of the oscillator.   b) Entrance to the radiator

Figure 40.   Phase-Space plot of the electrons as they a) exit the oscillator and b) enter the radiator of SELENE. The strength of the dispersive section is $D = 0.25$.

Using a variable strength for this dispersive section, from an achromatic bend for $a > 4$ to $D \approx 1$ for weak fields of $a \approx 1.5$ will allow for dynamic control to maximize bunching of the electrons prior to entering the radiator. This design meets the requirements of bunching the electrons for the radiator and reducing the optical field strength below the damage threshold of current mirror technology.

LIST OF REFERENCES

1. H.E. Bennett, et al., "Free-Electron Laser Power Beaming to Satellites at China Lake, California", Nuclear Instruments and Methods in Physics Research, A341, pp. 124-131,(1994).

2. R. Hartleib, et al., "Selene Site Study", Public Works, Facility Planning Division, Naval Air Weapons Station, China Lake, Appendix A (1994).

3. W.B. Zeleny, "Selected Topics in Electrodynamics", unpublished notes, pp. 24-40, (1993).

4. W.B. Colson, Free Electron Laser Handbook, eds. W.B. Colson, C. Pellegrini and A. Renieri (North-Holland, Amsterdam:1990), Chapter 5.

5. W. H. Beyer, CRC Standard Mathematical Tables 27th Edition, pp 352-355, (1984).

6. E. T. Scharlemann, Journal of Applied Physics, 58,2154, (1985).

7. W. B. Colson, "Self-Consistent Gain in the Optical-Klystron Free-Electron Laser", The American Physical Review A, pp 2353-2361, (1985).

8. J. B. Hall, "Simulations of an FEL Producing Coherent X-Rays Utilizing the SLAC Linac", MS Thesis, Naval Postgraduate School (1994).

9. D. Quick, "Simulations of the High Average Power SELENE Free Electron Laser Prototype", MS Thesis, Naval Postgraduate School (1994).

10. Dave Newnam, CST, Los Alamos Laboratories, personal communications, 24 May, 1995.

11. John Albertine, Director, Directed Energy Weapons Programs, Space and Naval Warfare Systems Command, personal communications, 25 May, 1995.

12. R.K. Wangsness, Electromagnetic Fields, John Wiley & Sons, Inc., p 417, (1979).

INITIAL DISTRIBUTION LIST

1. Defense Technical Information Center   2

    Cameron Station

    Alexandria, Virginia 22304-6145

2. Library, Code 52   2

    Naval Postgraduate School

    Monterey, California 93943-5002

3. Professor William B. Colson, Code PH/Cw   6

    Department of Physics

    Naval Postgraduate School

    Monterey, California 93943-5000

4. Professor Robert L. Armstead, Code PH/Ar   1

    Department of Physics

    Naval Postgraduate School

    Monterey, California 93943-5000

5. Doctor Harold E. Bennett   2

    Naval Air Warfare Center

    Weapons Division, Code C023103

    Research Department

    China Lake, California 93555

6. John Albertine   2

    Code 332, Division Director

    Directed Energy Division

    Space and Naval Warfare Systems Command

    2451 Crystal Drive

    Arlington, Virginia 22245-5200

7. Lieutenant Eric Kelsey, USN   2

    3447 19th Street

    Greeley, Colorado 80631